

---

# Conditional Sig-Wasserstein GANs for Time Series Generation

---

**Hao Ni**

Department of Mathematics  
University College London  
London, UK  
h.ni@ucl.ac.uk

**Lukasz Szpruch**

Department of Mathematics  
University of Edinburgh  
Edinburgh, UK  
lszpruch@turing.ac.uk

**Magnus Wiese**

Department of Mathematics  
University of Kaiserslautern  
Kaiserslautern, Germany  
wiese@rhrk.uni-kl.de

**Shujian Liao**

Department of Mathematics  
University College London  
London, UK  
shujian.liao.18@ucl.ac.uk

**Baoren Xiao**

Department of Mathematics  
University College London  
London, UK  
baoren.xiao.18@ucl.ac.uk

## Abstract

Generative adversarial networks (GANs) have been extremely successful in generating samples, from seemingly high dimensional probability measures. However, these methods struggle to capture the temporal dependence of joint probability distributions induced by time-series data. Furthermore, long time-series data streams hugely increase the dimension of the target space, which may render generative modelling infeasible. To overcome these challenges, we integrate GANs with mathematically principled and efficient path feature extraction called the signature of a path. The signature of a path is a graded sequence of statistics that provides a universal description for a stream of data, and its expected value characterises the law of the time-series model. In particular, we develop a new metric, (conditional) Sig- $W_1$ , that captures the (conditional) joint law of time series models, and use it as a discriminator. The signature feature space enables the explicit representation of the proposed discriminators which alleviates the need for expensive training. Furthermore, we develop a novel generator, called the conditional AR-FNN, which is designed to capture the temporal dependence of time series and can be efficiently trained. We validate our method on both synthetic and empirical dataset and observe that our method consistently and significantly outperforms state-of-the-art benchmarks with respect to measures of similarity and predictive ability.

## 1 Introduction

Time-series data streams are often not stationary, which means that one may only have a relative small sample sets of data with the same joint probability distribution. In addition there are only a few data points far out in the tails of the probability distribution (e.g financial crash, pandemic), which makes robust training of data hungry algorithms infeasible. It is therefore critical to research methods for synthesising time-series datasets that exhibit the same properties as the real data. Such synthetic datasets can facilitate testing and validation of data-driven products and enable data sharing by respecting the demand for privacy constraints. See [1, 2] for the overview of the applications and challenges for synthetic data generation.

## 1.1 Generative model for time series

Let  $\nu$  be an unknown target distribution. Consider a sequence of  $N$  data points  $x_{1:N}$  in  $\mathcal{X} \subseteq \mathbb{R}^d$  from  $\nu$ . The aim of the generative model is to map samples from some basic distribution  $\mu_z$  supported on  $\mathcal{Z} \subseteq \mathbb{R}^{d_z}$  into samples from  $\nu$ . More precisely, given latent  $(\mathcal{Z}, \mathcal{B}(\mathcal{Z}))$  and target  $(\mathcal{X}, \mathcal{B}(\mathcal{X}))$  measure spaces one considers a map  $G : \Theta^{(g)} \times \mathcal{Z} \rightarrow \mathcal{X}$ , with  $\Theta^{(g)}$  being a parameter space that, given parameters  $\theta \in \Theta^{(g)}$ , transports  $\mu_z$  into  $G_{\#}^{\theta} \mu_z = \mu_z((G^{\theta})^{-1}(B))$ ,  $B \in \mathcal{B}(\mathcal{X})$ . The aim is to find  $\theta$  such that  $G_{\#}^{\theta} \mu_z$  is a good approximation of  $\nu$  with respect to a suitable metric. The optimal transport metrics, such as the Wasserstein distance, are a popular choice due to the ability to capture meaningful geometric features between measures even when their supports do not overlap but are expensive to compute. Maximum Mean Discrepancy (MMD) metrics are much cheaper to compute but their utility hinges on the choice of the kernel [3].

For time-series generation, learning the conditional distribution is often more desirable than learning joint law. Indeed for predictive modelling, one is interested in conditional distribution  $\nu(\cdot | x_{past})$  of the future time series  $x_{future} := x_{t+1:t+q}$  given the past time series  $x_{past} := x_{t-p+1:t}$ . Learning such conditional distributions is particularly important in the case when a series  $x_{1:N}$  comes from a non-stationary distribution and learning conditional laws is more efficient and requires less data [4]. It has been observed in [5, 6] that unconditional GANs are not fit to generate the conditional distribution of the future time series based on the past time-series information. However, the challenge in developing conditional integrated probability metrics is that conditional expectations are difficult to compute and standard statistical approximation methods do not scale well with the dimension. Additional difficulty in generating time-series data is the dimension of the problem. Indeed joint distributions are supported on  $\mathbb{R}^{N \times d}$ . Hence, for long time-series data streams this hugely increases the dimension of the problem at hand making synthetic time-series data generator highly non-trivial.

## 1.2 Our contributions

In this work, we combine classical GANs with an efficient path feature extraction method called the signature of a path. The signature of a path is a mathematical object that emerges from rough-path theory and provides a highly abstract and universal description of complex multimodal data streams that has recently demonstrated great success in several machine learning tasks [7, 8, 9]. Furthermore, by working with the signature of a path one can design algorithms that are robust with respect to missing data points or datasets that are not uniformly distributed across the time dimension [10]. Importantly, the signature preserves the order of data and captures relevant structural/geometric properties. In this paper, we propose a generic SigCWGAN framework for training conditional generators. More precisely:

- **Discriminator:** We develop a novel (conditional) Sig- $W_1$  metric for distributions on the path space. By taking advantage of the signature feature space, Sig- $W_1$  has an explicit solution and does not require costly computation needed for the classical Wasserstein metric [11]. The ability of Sig- $W_1$  metric to capture the (conditional) distribution over the path space means that the generator trained with respect to this metric is generic in a sense that it will generalise well with respect to other metrics used in time-series analysis, such as the auto-correlation function (ACF), which we confirm empirically in section 5. This stands in contrast to the majority of the results in literature that evaluate the generators with respect to a specific criteria e.g. classification. For the conditional variant of C-Sig- $W_1$ , we leverage the universality of the signature representation and reduce the computation of conditional expectations to a simple linear regression problem yielding an explicit solution to C-Sig- $W_1$ .
- **Generator:** We build an AR-FNN that maps the past time-series and noise vectors into the future time-series. Our generators by construction capture the auto-regressive nature of time-series.

## 1.3 Literature Review

The literature on the generative models is in abundance and here we focus on works who specifically tackled time-series data generation. Inspired by the recent success of generative adversarial networks (GANs), [12] present Quant GANs, consisting of a generator and discriminator which utilise temporal convolutional networks (TCNs). Quant GANs can well capture the temporal dependence of time

series, such as volatility clustering; Kondratyev et al.[13] used Restricted Boltzmann Machine (RBM) to build a generator of synthetic market data and reported good performance in particular due to high regularisation. A variant of Conditional GANs has been proposed in [14] to generate order flow in the limit order book. Conditional GANs have also been considered in [15, 16, 17, 18] for univariate and in [19, 20, 21] for multivariate time-series generation. Henry-Labordere in [22, 23] proposed several algorithms for data generation using dual and primal-dual representations for optimal transport metrics. His algorithms achieved good performance for 6-dimensional time-series data. The combination of signatures, genetic algorithms and autoencoders has been developed in [24]. The importance of including the correct prior when training GANs for time series data has been suggested in [5]. There authors develop a novel Time-series GAN algorithm that significantly outperforms classical GAN.

#### 1.4 Outline of the paper.

In section 2, we introduce the signature of a path and review its properties. Then we proceed to propose the Sig- $W_1$  metric on measures on the path space by combining  $W_1$  metric and the signature feature map in section 3. In section 4, we propose a novel signature-based framework for time-series generation, which uses the AR-FNN network as a conditional generator and the conditional Sig- $W_1$  metric as a discriminator. Finally, we present our numerical results in section 5 and outline the direction of our future work in section 6.

## 2 The Signature and Expected Signature of Data Streams

In this section, we give a brief introduction to the signature feature of a path and expected signature of a stochastic process, which can characterise the law on the stochastic process and can be thought of a moment generating function on the path space. The rigorous and thorough introduction of the signature feature set for un-parameterized paths can be found in [25, 26, 27]. For simplicity, we restrict the discussion to the space of continuous functions mapping from a compact time interval  $J$  to  $\mathbb{R}^d$  with finite  $p$ -variation and starting from the origin, denoted by  $\mathcal{C}_0^p(J, \mathbb{R}^d)$ .

### 2.1 The Signature of a Path

Let  $T((\mathbb{R}^d)) := \bigoplus_{k=0}^{\infty} (\mathbb{R}^d)^{\otimes k}$  be a tensor algebra space (c.f supplementary material A), where the signature of a  $\mathbb{R}^d$ -valued path takes value.

**Definition 2.1** (Signature). *Let  $X \in \mathcal{C}_0^p(J, \mathbb{R}^d)$  such that the following integration makes sense. The signature of the path  $X$  is defined as  $S(X_J) = (1, X_J^1, \dots, X_J^k, \dots) \in T((\mathbb{R}^d))$ , where*

$$X_J^k = \int_{t_1 < t_2 < \dots < t_k, t_1, \dots, t_k \in J} dX_{t_1} \otimes \dots \otimes dX_{t_k}. \quad (1)$$

Let  $S_M(X_J)$  denote the truncated signature of  $X$  of degree  $M$ , i.e.  $S_M(X_J) = (1, X_J^1, \dots, X_J^M)$ .

For  $p \in [1, 2)$ , the integration is defined as the Young's integral. When  $X$  is a piecewise linear path of finite pieces, the signature of  $X$  can be computed explicitly and we use the open source python package signatory [28], which supports PyTorch [29], to do it.

The signature of a path provides a top-down description of the path; low order terms of the signature capture the global description of the path and higher order term gives more information on the local structure of the path. Let  $J = [s, t]$ . The first level of the signature  $X_J^1$  is the increment of the path  $X_t - X_s$ , and the second level of the signature  $X_J^2$  includes the information of the area enclosed by  $X$  and the chord connecting the end and start points of  $X$ .  $X_J^k$  has the dimension  $d^k$ , and thus the dimension of the truncated signature of  $S_M(X_J)$  is  $\frac{d^{M+1}-1}{d-1}$ .

Let  $\Omega_0^1(J, \mathbb{R}^d)$  denote the space of time augmented paths, i.e.  $\Omega_0^1(J, \mathbb{R}^d) = \{t \mapsto (t, x_t) | x \in \mathcal{C}_0^1(J, \mathbb{R}^d)\}$ . For any discrete time series  $X := (X_{t_i})_{i=1}^L$ , we follow Definition 4.3 [27] to augment time dimension and embed it to  $\bar{X} \in \Omega_0^1(J, \mathbb{R}^d)$ .

The following properties make the signature an excellent candidate for the feature of data streams:

- **Universality.** Non-linear continuous functions of the un-parameterized data streams are universally approximated by linear functionals in the signature space [27]. More precisely, we have the following result:

**Theorem 2.1.** *Consider a compact set  $K \subset \Omega_0^1(J, \mathbb{R}^d)$ . Denote by  $S$  the function that maps a path  $X$  from  $K$  to its signature  $S(X)$ . Let  $f : K \rightarrow \mathbb{R}$  be any continuous function. Then, for any  $\epsilon > 0$ , there exists  $M > 0$ , and a linear functional  $L$  acting on the truncated signature of degree  $M$  such that*

$$\sup_{X \in K} |f(X) - \langle L, S_M(X) \rangle| < \epsilon \quad (2)$$

The theorem tells us that any continuous functional on the paths can be arbitrarily well approximated by a linear combination of coordinate signatures.

- **Uniqueness.** The signature of a path determines the path up to time parameterization[30, 31]. More specifically, when restricted the path space to  $\Omega_0^1(J, \mathbb{R}^d)$ , the signature map is bijective. In other words, the signature of a path in  $\Omega_0^1(J, \mathbb{R}^d)$  determines the path completely.

Moreover, the signature of a path takes the functional view on the time-series data by lifting discrete time series to a continuous path by interpolation. Therefore, it allows the unified treatment on irregular time series (e.g. variable length, missing data, asynchronous multi-dimensional data) to the path space [26].

## 2.2 Expected Signature of a Stochastic Process

Let  $X$  denote a stochastic process defined on a probability space. Suppose that Equation (1) is well defined for  $X$  a.s., and thus the signature of  $X$  is a random variable in  $T((\mathbb{R}^d))$ . Assume that the expectation of  $S(X)$  is finite, we define the expected signature of the stochastic process  $X$ . By Proposition 6.1 in [32], we have the following result:

**Theorem 2.2.** *Let  $X$  and  $Y$  be two  $\Omega_0^1(J, \mathbb{R}^d)$ -valued random variables. If  $\mathbb{E}[S(X)] = \mathbb{E}[S(Y)]$ , and  $\mathbb{E}[S(X)]$  has infinite radius of convergence, then  $X = Y$  in the distribution sense.*

In other words, under the regularity condition, the distribution  $\mu$  on the path space is characterized by  $\mathbb{E}_{X \sim \mu}[S(X)]$ . Intuitively, the signature of a path plays a role of a non-communicate polynomial on the path space. Therefore the expected signature of a random process can be viewed as an analogy of the moment generating function of a  $d$ -dimensional random variable. For example, the expected Stratonovich signature of Brownian motion determines the law of the Brownian motion [33].

## 3 The Signature Wasserstein-1 metric (Sig- $W_1$ ) and Sig-MMD

We propose a new Signature Wasserstein-1 (Sig- $W_1$ ) metric on the measures on the path space  $\mathcal{X} = \Omega_0^1(J, \mathbb{R}^d)^1$  by combining the signature feature and the Wasserstein-1 ( $W_1$ ) metric. Let  $\mu$  and  $\nu$  be two measures on the path space  $\mathcal{X}$  with a compact support  $K$ . The Kantorovich and Rubinstein dual representation of Wasserstein-1 metric is given by

$$W_1(\mu, \nu) = \sup \left\{ \int f(x) d(\mu - \nu)(x) \mid \text{continuous } f : \mathcal{X} \rightarrow \mathbb{R}, \text{Lip}(f) \leq 1 \right\}, \quad (3)$$

where  $\text{Lip}(f)$  denotes the Lipschitz constant of  $f$ . From this definition and the universality of the signature map stated in Theorem 2.1, it is natural to embed the path to the signature space and consider the distance between  $\mu$  and  $\nu$  by

$$\text{Sig-}W_1(\mu, \nu) := \sup_{|L| \leq 1, L \text{ is a linear functional}} L(\mathbb{E}_\mu[S(X)] - \mathbb{E}_\nu[S(X)]), \quad (4)$$

where  $\mathbb{E}_\mu$  and  $\mathbb{E}_\nu$  are the expectation taken under  $\mu$  and  $\nu$  respectively. Hence, we see that by working with the signature feature space one can reduce the nonlinear optimisation of computing  $W_1$  distance over the class of Lipschitz functionals to the linear one over the *linear* functionals on the signature

<sup>1</sup>We focus on the path space  $\Omega_0^1(J, \mathbb{R}^d)$ , as any discrete time series can be embedded to this path space.

space. Due to the factorial decay of the signature (Lemma A.1), we can approximate Equation (4) by using the truncated signature up to a finite degree  $M$ , i.e.

$$\text{Sig-}W_1^{(M)}(\mu, \nu) := \sup_{|L| \leq 1, L \text{ is a linear functional}} L(\mathbb{E}_\mu[S_M(X)] - \mathbb{E}_\nu[S_M(X)]), \quad (5)$$

When the norm of  $L$  is chosen as the  $l_2$  norm of the linear coefficients of  $L$ , this reduced optimization problem admits the analytic solution

$$\text{Sig-}W_1^{(M)}(\mu, \nu) = |\mathbb{E}_\mu[S_M(X)] - \mathbb{E}_\nu[S_M(X)]|, \quad (6)$$

where  $|\cdot|$  is  $l_2$  norm (see Lemma A.3). We call (6) the truncated Sig- $W_1$  metric of degree  $M$ . In [34], if one chooses the truncated signature up to degree  $M$  as the feature map, then the corresponding Maximum Mean Discrepancy (Sig-MMD) is the square of  $\text{Sig-}W_1^{(M)}(\mu, \nu)$ .

## 4 The Signature-based Conditional Generator (SigCWGAN)

Motivated by the autoregressive type models in time series literature, we assume that a  $\mathbb{R}^d$ -valued time series  $(X_t)_{t=1}^T$  satisfies  $X_{t+1} = f(X_{t-p+1:t}) + \varepsilon_t$ , where  $\mathbb{E}[\varepsilon_{t+1}|\mathcal{F}_t] = 0$ ,  $\mathcal{F}_t$  is the information up to time  $t$  and  $f: \mathbb{R}^{p \times d} \rightarrow \mathbb{R}^d$  is a continuous but unknown function. The objective of the Signature-based Conditional Generator for time series (SigCWGAN) is to generate the joint distribution of the future time series  $x_{\text{future}} = X_{t:t+q}$  given the past time series  $x_{\text{past}} = X_{t-p+1:t}$ . The following analysis holds for any method of embedding a discrete time series to a path as long as its signature can uniquely determine the path; for example, we can embed any discrete time series  $x$  as a time augmented path in  $\Omega_0^1(J, \mathbb{R}^d)$  defined before.

### 4.1 The Conditional AR-FNN Generator

The conditional generator  $G^\theta: \mathbb{R}^{d \times p} \times \mathcal{Z} \rightarrow \mathbb{R}^d$ , which aims to take the past path ( $X_{t-p+1:t} = x$ ) and the noise vector  $Z_{t+1}$  to generate a random variable in  $\mathbb{R}^d$  whose conditional distribution of the next step forecast is as close as possible to  $\mathbb{P}(X_{t+1}|X_{t-p+1:t} = x)$ . Here  $\mathcal{Z} = \mathbb{R}^d$  and  $(Z_t)_t$  are iid with the standard normal distribution. Here the AR-FNN generator  $G^\theta$  is chosen to be a feedforward neural network, residual connections [35] and parametric ReLUs as activation functions [36] (see subsection A.4 for a detailed description). Given  $X_{t-p+1:t}$ , we estimate the next step estimator  $\hat{X}_{t+1}^{(t)} = G^\theta(X_{t-p+1:t}, Z_{t+1})$ . Then we use the next step estimator  $\hat{X}_{t+1}^{(t)}$  to generate the step-2 estimator by  $\hat{X}_{t+2}^{(t)} = G^\theta(X_{t-p+2:t}, \hat{X}_{t+1}^{(t)}, Z_{t+2})$ . To predict the  $i$ -step estimator at each time  $t$ , we update the conditioning variable by inserting  $\hat{X}_{t+i-1}^{(t)}$  to the end of the previous conditioning variable in a sliding window fashion. By repeating this procedure for  $q$  steps, we obtain the step- $q$  estimator  $\hat{X}_{t+1:t+q}^{(t)}$  (See Algorithm 1 in Supplementary Material).

The proposed AR-FNN generator is designed to capture the autoregressive structure of the target time series by construction. We use the lagged  $p$  values as the conditioning variable for the AR-FNN generator and the simple forward neural network to achieve impressive resemblance of temporal dependence to real time series.

### 4.2 The Conditional Sig- $W_1$ Discriminator

Given two conditional distributions of  $\mu(X_{\text{future}}|x_{\text{past}})$  and  $\nu(X_{\text{future}}|x_{\text{past}})$ , we aim to test whether they are the same in the sense that when  $x_{\text{past}} = x$  is fixed and quantify the distance between them. Similarly to the unconditional case, we define the truncated conditional Signature Wasserstein-1 metric of degree  $M$  denoted by C-Sig- $W_1^{(M)}$  on  $\mu$  and  $\nu$  as the  $l_2$  norm of the difference between two conditional expected signatures up to degree  $M$ , i.e.

$$\text{C-Sig-}W_1^{(M)}(\mu, \nu) := |\mathbb{E}_\mu[S_M(X_{\text{future}})|x_{\text{past}} = x] - \mathbb{E}_\nu[S_M(X_{\text{future}})|x_{\text{past}} = x]|.$$

Therefore, we define the loss function as the summation of the  $l_2$  norm of the error between the conditional expected signature of future true path and future path generated by the generator given the past path over each time  $t$ , i.e.

$$L(\theta) = \sum_t |\mathbb{E}_\mu[S_M(X_{t+1:t+q})|X_{t-p+1:t}] - \mathbb{E}_\nu[S_M(\hat{X}_{t+1:t+q}^{(t)})|X_{t-p+1:t}]|, \quad (7)$$

where  $\nu$  and  $\mu$  denote the conditional distribution induced by the real data and synthetic generator respectively,  $G^\theta$  is the generator,  $\hat{X}_{t+1:t+q}^{(t)}$  is the  $q$ -step forecast generated by  $G^\theta$ .

### 4.3 SigCWGAN Algorithm

We are ready to present the SigCWGAN algorithm based on the proposed conditional generator/discriminator. The flowchart of SigCWGAN algorithm is given in Figure 1.

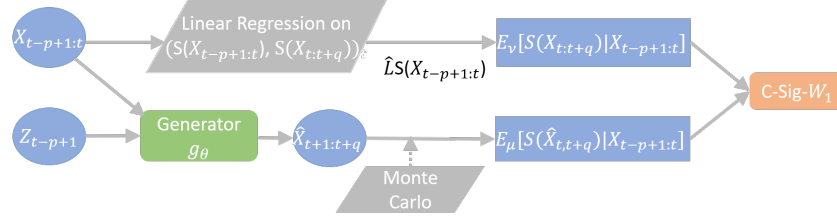


Figure 1: The illustration of the flowchart of SigCWGAN.

First, we estimate  $\mathbb{E}_\nu[S_M(X_{t:t+q})|X_{t-p+1:t}]$  accurately from the true data. Based on the autoregressive assumption of  $X$ , the conditional expected signature of  $X_{t+1:t+q}$  given  $x_{t-p+1:t} = x$  does not depend on  $t$ , which allows us to use the supervised learning algorithm to learn from true data.

By embedding the past path in the signature space, [27] shows that this non-linear supervised learning problem can be reduced to a linear regression on the truncated signature of the past path. Thus we apply the linear regression on  $(S_N(X_{t-p+1:t}), S_M(X_{t+1:t+q}))_t$  and obtain the estimator of the linear functional  $\hat{L}$ . We use  $\hat{L}(S_N(X_{t-p+1:t}))$  as an estimator for  $\mathbb{E}_\nu[S_M(X_{t+1:t+q})|X_{t-p+1:t}]$ .

Given  $X_{t-p+1:t}$ , we sample the noise from the distribution of the latent process  $Z_{t+1:t+q}$  and generate a trajectory  $\hat{X}_{t+1:t+q}^{(t)}$  by  $G^\theta$ . By Monte-Carlo method we can get the reliable estimator for  $\mathbb{E}_\mu[S(\hat{X}_{t+1:t+q}^{(t)})|X_{t-p+1:t}]$ . We compute the loss function based on Equation (7) and update the model parameters of the generator  $G^\theta$  by the stochastic gradient descent algorithm. The pseudocode of SigCWGAN is listed in Algorithm 2 in Supplementary Material.

## 5 Numerical Experiments

To benchmark with SigCWGAN, we choose three representative generative models for the time-series generation, i.e. (1) TimeGAN [5], (2) RCGAN [37] - a conditional GAN and (3) GMMN [38] - an unconditional MMD with Gaussian kernel. To assess the goodness of the fitting of a generative model, we consider three main criteria (a) the marginal distribution of time series; (b) the temporal and feature dependence; (c) the usefulness[5] - synthetic data should be as useful as the real data when used for the same predictive purposes (i.e. train-on-synthetic, test-on-real). The test metrics are defined below.

**Metric on marginal distribution:** We compute the empirical probability density function (epdf) of the real time series and synthetic data using the histogram. We take the absolute difference of those two epdfs as the metric on marginal distribution averaged over feature dimension.

**Metric on dependency :** We use the absolute error of the auto-correlation estimator by real data and synthetic data as the metric to assess the temporal dependency. For  $d > 1$ , we use the  $l_1$  norm of the difference between cross correlation matrices.

**$R^2$  comparison:** Following [17] and [5], we consider the problem of predicting next-step temporal vectors using the lagged values of time series using the real data and synthetic data. First we train a supervised learning model on real data and evaluate the trained model on the real data in terms of  $R^2$ (TRTR). Then we train the same supervised learning model on synthetic data and compute  $R^2$  of the trained model on the true data (TSTR). The closer two  $R^2$  are, the better generative model it is.

The Supplementary Material contains the precise definitions of test metrics, additional information on implementation details of SigCWGAN and numerical results of VAR(1) data, ARCH(1) data and

empirical data. Implementation of SigCWGAN can be found in <https://github.com/SigCGANs/Conditional-Sig-Wasserstein-GANs>.

### 5.1 Synthetic data generated by Vector Autoregressive Model

To demonstrate the model’s ability to generate realistic multi-dimensional time series in a controlled environment, we consider synthetic data generated by the Vector Autoregressive (VAR) model, which is a key illustrative example in TimeGAN [5]. In the  $d$ -dimensional VAR(1) model time series are defined recursively for  $t \in \{1, \dots, T-1\}$  through  $X_{t+1} = \phi X_t + \epsilon_{t+1}$ , where  $(\epsilon_t)_{t=1}^T$  are iid Gaussian-distributed random variables with co-variance matrix  $\sigma \mathbf{1} + (1 - \sigma)\mathbf{I}$ ;  $\mathbf{I}$  is a  $d \times d$  identity matrix. Here, the coefficient  $\phi \in [-1, 1]$  controls the auto-correlation of the time series and  $\sigma \in [0, 1]$  the correlation of the  $d$  features.

In our benchmark, we investigate the dimensions  $d = 1, 2, 3$  and various  $(\sigma, \phi)$ . Across all dimensions we observe that the SigCWGAN has a comparable performance or outperforms the baseline models in terms of the metrics defined above. Furthermore, we find that as the dimension increases the performance of SigCWGANs exceeds baselines. We illustrate this finding in Figure 2(Right) which shows the relative error of TSTR  $R^2$  when varying the dimensionality of VAR(1). Observe that the SigCWGAN remains a very low relative error, but the performance of the other models deteriorate significantly, especially the GMMN.

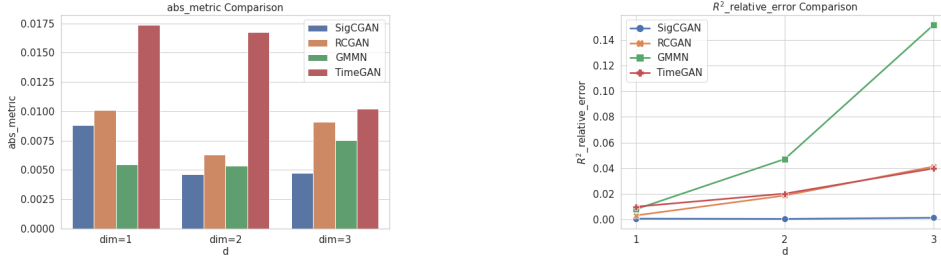


Figure 2: (Left) The distributional metric (abs\_metrics) comparison; (Right) the  $R^2$  (TSTR) comparison. VAR(1) data is generated for  $\phi = 0.8$  and  $\sigma = 0.8$ .

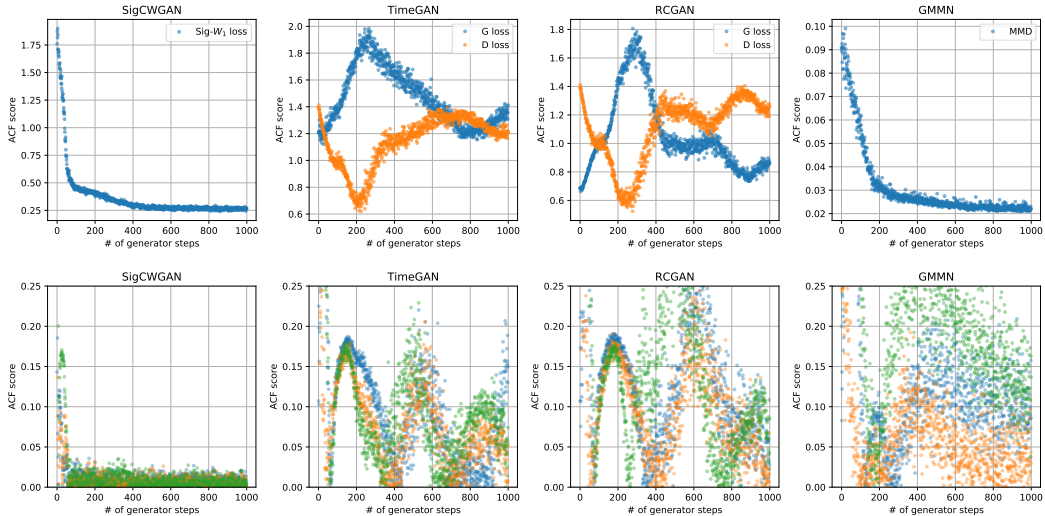


Figure 3: (Upper panel) Evolution of the training loss functions. (Lower panel) Evolution of the ACF scores. Each colour represents the ACF score of one dimension. Results are for the 3-dimensional VAR(1) model for  $\phi = 0.8$  and  $\sigma = 0.8$ .

Figure 3 shows the development of the ACF scores through the course of training for the 3-dimensional VAR(1) model. While the ACF scores of the baseline models oscillate heavily, the SigCWGAN

ACF score and Sig- $W_1$  distance converge nicely towards zero. Also, the MMD loss converges nicely towards zero. However, in contrast the ACF scores do not converge. This highlights the stability and usefulness of the Sig- $W_1$  distance as a loss function.

Furthermore, the SigCWGAN has the advantage of generating the realistic long time series over the other models, which is reflected by that the marginal density function of a synthetic sampled path of 80,000 steps is much closer to that of real data than baselines in Figure 4.

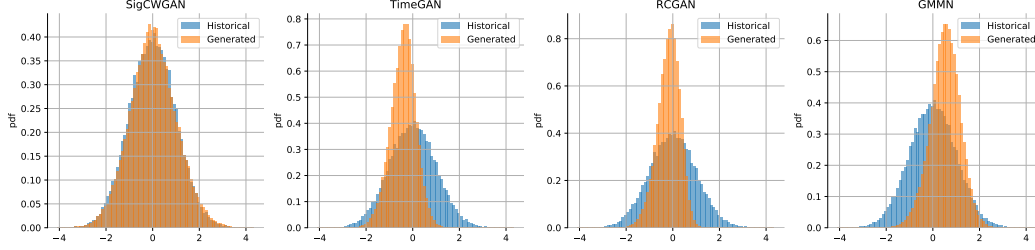


Figure 4: Comparison of the marginal distributions of one long sampled path (80,000 steps) with the real distribution.

## 5.2 Empirical Data

To assess the performance of our method on the empirical data, we choose the dataset of the S&P 500 index (SPX) and Dow Jones index (DJI) and their realized volatility, which is retrieved from the Oxford-Man Institute's "realised library"[39]. We aim to generate a time series of both the log return of the close prices and the log of median realised volatility of (a) the SPX only; (b) the SPX and DJI. Table 1 shows that SigCWGAN achieves the superior or comparable performance to the other baselines. The SigCWGAN generates the realistic synthetic data of the SPX and DJI data shown by the marginal distribution comparison with that of real data in Figure 5. For the SPX only data, GMMN performs slightly better than our model in terms of the fitting of lag-1 auto-correlation and marginal distribution ( $\leq 0.0013$ ), but it suffers from the poor predictive performance and feature correlation in Table 1. When the SigCWGAN is outperformed, the difference is negligible. Furthermore, the test metrics, i.e. the ACF loss and density metric, of our model are evolving much smoother than the test metrics of the other baseline models shown in Figure 13.

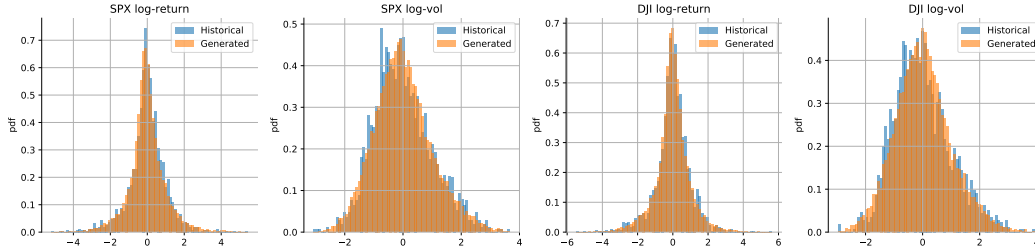


Figure 5: Comparison of the marginal distributions of the generated SigCWGAN paths and the SPX and DJI data.

Metrics	marginal distribution	auto-correlation	correlation	$R^2(\%)$	Sig- $W_1$
SigCWGAN	0.01730, 0.01674	0.01342, <b>0.01192</b>	<b>0.01079</b> , <b>0.07435</b>	2.996, 7.948	<b>0.18448</b> , <b>4.36744</b>
TimeGAN	0.02155, 0.02127	0.05792, 0.03035	0.12363, 0.61488	5.955, 8.586	0.58541, 5.99482
RCGAN	0.02094, <b>0.01655</b>	0.03362, 0.04075	0.04606, 0.15353	<b>2.788</b> , <b>7.190</b>	0.47107, 5.43254
GMMN	<b>0.01608</b> , 0.02387	<b>0.01283</b> , 0.02676	0.04651, 0.22380	9.049, 7.384	0.59073, 6.23777

Table 1: Numerical results of the stock datasets. In each cell, the left/right number are the result for the SPX data/ the SPX and DJI data respectively. We use the relative error of TSTR  $R^2$  against TRTR  $R^2$  as the  $R^2$  metric.



## 6 Conclusion

In this paper, we developed the conditional Sig-Wasserstein GAN for time series generation based on the explicit approximation of  $W_1$  metric using the signature features space. This eliminates the problem of having to approximate a costly critic / discriminator and, as a consequence, dramatically simplifies training. Our method achieves state-of-the-art results on both synthetic and empirical dataset.

## Broader Impact

We have introduced a new tool for generating time series. As with any tool, it may be used in both positive and negative ways. The authors have a particular interest in applying the developed methodology for training, testing and validating machine learning algorithms and also for enabling data sharing of priority data with a wider research community.

## Acknowledgments and Disclosure of Funding

HN is supported by the EPSRC under the program grant EP/S026347/1. HN and LS are supported by the Alan Turing Institute under the EPSRC grant EP/N510129/1.

## References

- [1] Samuel Assefa, Danial Dervovic, Mahmoud Mahfouz, Tucker Balch, Prashant Reddy, and Manuela Veloso. Generating synthetic data in finance: opportunities, challenges and pitfalls.
- [2] Steven M Bellovin, Preetam K Dutta, and Nathan Reiting. Privacy and synthetic datasets. *Stan. Tech. L. Rev.*, 22:1, 2019.
- [3] Aude Genevay, Lénaïc Chizat, Francis Bach, Marco Cuturi, and Gabriel Peyré. Sample complexity of sinkhorn divergences. *arXiv preprint arXiv:1810.02733*, 2018.
- [4] Andrew Y Ng and Michael I Jordan. On discriminative vs. generative classifiers: A comparison of logistic regression and naive bayes. In *Advances in neural information processing systems*, pages 841–848, 2002.
- [5] Jinsung Yoon, Daniel Jarrett, and Mihaela van der Schaar. Time-series generative adversarial networks. In *Advances in Neural Information Processing Systems*, pages 5509–5519, 2019.
- [6] Yong Ren, Jun Zhu, Jialian Li, and Yucen Luo. Conditional generative moment-matching networks. In *Advances in Neural Information Processing Systems*, pages 2928–2936, 2016.
- [7] Zecheng Xie, Zenghui Sun, Lianwen Jin, Hao Ni, and Terry Lyons. Learning spatial-semantic context with fully convolutional recurrent network for online handwritten chinese text recognition. *IEEE transactions on pattern analysis and machine intelligence*, 40(8):1903–1917, 2017.
- [8] Weixin Yang, Terry Lyons, Hao Ni, Cordelia Schmid, Lianwen Jin, and Jiawei Chang. Leveraging the path signature for skeleton-based human action recognition. *arXiv preprint arXiv:1707.03993*, 2017.
- [9] Patrick Kidger, Patric Bonnier, Imanol Perez Arribas, Cristopher Salvi, and Terry Lyons. Deep signature transforms. In *Advances in Neural Information Processing Systems*, pages 3099–3109, 2019.
- [10] Patrick Kidger, James Morrill, James Foster, and Terry Lyons. Neural controlled differential equations for irregular time series. *arXiv preprint arXiv:2005.08926*, 2020.
- [11] Gabriel Peyré, Marco Cuturi, et al. Computational optimal transport. *Foundations and Trends® in Machine Learning*, 11(5-6):355–607, 2019.
- [12] Magnus Wiese, Robert Knobloch, Ralf Korn, and Peter Kretschmer. Quant gans: deep generation of financial time series. *Quantitative Finance*, pages 1–22, 2020.
- [13] Alexei Kondratyev and Christian Schwarz. The market generator. *Available at SSRN*, 2019.

- [14] Junyi Li, Xintong Wang, Yaoyang Lin, Arunesh Sinha, and Michael P Wellman. Generating realistic stock market order streams. 2018.
- [15] Chris Donahue, Julian J. McAuley, and Miller Puckette. Adversarial audio synthesis. In *ICLR*, 2019.
- [16] Jesse Engel, Kumar Krishna Agrawal, Shuo Chen, Ishaan Gulrajani, Chris Donahue, and Adam Roberts. Gansynth: Adversarial neural audio synthesis. *ArXiv*, abs/1902.08710, 2019.
- [17] Cristóbal Esteban, Stephanie L. Hyland, and Gunnar Rätsch. Real-valued (medical) time series generation with recurrent conditional gans, 2017.
- [18] Adriano Koshiyama, Nick Firoozye, and Philip Treleaven. Generative adversarial networks for financial trading strategies fine-tuning and combination. *arXiv preprint arXiv:1901.01751*, 2019.
- [19] Rao Fu, Jie Chen, Shutian Zeng, Yiping Zhuang, and Agus Sudjianto. Time series simulation by conditional generative adversarial net. *arXiv preprint arXiv:1904.11419*, 2019.
- [20] Alireza Koochali, Andreas Dengel, and Sheraz Ahmed. If you like it, gan it. probabilistic multivariate times series forecast with gan. *arXiv preprint arXiv:2005.01181*, 2020.
- [21] Magnus Wiese, Lianjun Bai, Ben Wood, and Hans Buehler. Deep hedging: Learning to simulate equity option markets. *SSRN Electronic Journal*, 2019.
- [22] Pierre Henry-Labordere. (martingale) optimal transport and anomaly detection with neural networks: A primal-dual algorithm. *Available at SSRN 3370910*, 2019.
- [23] Pierre Henry-Labordere. Generative models for financial data. *Available at SSRN 3408007*, 2019.
- [24] I. Perez Arribaz T. Lyons . Buehler, B. Hovarth and B. Wood. A data-driven market simulator for small data environments. *in preperation*, 2020.
- [25] Terry Lyons. Rough paths, signatures and the modelling of functions on streams. *arXiv preprint arXiv:1405.4537*, 2014.
- [26] Ilya Chevyrev and Andrey Kormilitzin. A primer on the signature method in machine learning. *arXiv preprint arXiv:1603.03788*, 2016.
- [27] Daniel Levin, Terry Lyons, and Hao Ni. Learning from the past, predicting the statistics for the future, learning an evolving system. *arXiv preprint arXiv:1309.0260*, 2013.
- [28] Patrick Kidger and Terry Lyons. Signatory: differentiable computations of the signature and logsignature transforms, on both CPU and GPU. *arXiv:2001.00706*, 2020.
- [29] Adam Paszke, Sam Gross, Francisco Massa, Adam Lerer, James Bradbury, Gregory Chanan, Trevor Killeen, Zeming Lin, Natalia Gimelshein, Luca Antiga, et al. Pytorch: An imperative style, high-performance deep learning library. In *Advances in Neural Information Processing Systems*, pages 8024–8035, 2019.
- [30] B.M. Hambly and Terry Lyons. Uniqueness for the signature of a path of bounded variation and the reduced path group. *Annals of Mathematics*, 171(1):109–167, 2010.
- [31] Horatio Boedihardjo and Xi Geng. The uniqueness of signature problem in the non-markov setting. *arXiv preprint arXiv:1401.6165*, 2014.
- [32] Ilya Chevyrev, Terry Lyons, et al. Characteristic functions of measures on geometric rough paths. *The Annals of Probability*, 44(6):4049–4082, 2016.
- [33] Terry Lyons, Hao Ni, et al. Expected signature of brownian motion up to the first exit time from a bounded domain. *The Annals of Probability*, 43(5):2729–2762, 2015.
- [34] Ilya Chevyrev and Harald Oberhauser. Signature moments to characterize laws of stochastic processes. *arXiv preprint arXiv:1810.10971*, 2018.
- [35] Kaiming He, Xiangyu Zhang, Shaoqing Ren, and Jian Sun. Deep residual learning for image recognition. In *Proceedings of the IEEE conference on computer vision and pattern recognition*, pages 770–778, 2016.
- [36] Kaiming He, Xiangyu Zhang, Shaoqing Ren, and Jian Sun. Delving deep into rectifiers: Surpassing human-level performance on imagenet classification. In *Proceedings of the IEEE international conference on computer vision*, pages 1026–1034, 2015.

- [37] Stephanie Hyland, Cristóbal Esteban, and Gunnar Rätsch. Real-valued (medical) time series generation with recurrent conditional gans. 2018.
- [38] Yujia Li, Kevin Swersky, and Rich Zemel. Generative moment matching networks. In *International Conference on Machine Learning*, pages 1718–1727, 2015.
- [39] Gerd Heber, Asger Lunde, Neil Shephard, and Kevin Sheppard. Oxford-man institute’s realized library, version 0.3, 2009.
- [40] Terry J Lyons, Michael Caruana, and Thierry Lévy. *Differential equations driven by rough paths*. Springer, 2007.
- [41] Diederik P Kingma and Jimmy Ba. Adam: A method for stochastic optimization. *arXiv preprint arXiv:1412.6980*, 2014.
- [42] Martin Heusel, Hubert Ramsauer, Thomas Unterthiner, Bernhard Nessler, and Sepp Hochreiter. Gans trained by a two time-scale update rule converge to a local nash equilibrium. In *Advances in neural information processing systems*, pages 6626–6637, 2017.

## A Supplementary Material

### A.1 Preliminary

For the sake of precision, we start by introducing basic concepts around the signature of a path, which lays the foundation for our analysis on the signature approximation for Wasserstein-1 Distance. Besides, we give a brief introduction to Maximum Mean Discrepancy (MMD) in this subsection.

#### A.1.1 Tensor algebra space

The tensor algebra space of  $E$  is where the signature of a  $E$ -valued path take values. For simplicity, fix  $E = \mathbb{R}^d$ . Then  $E$  has the basis  $\{e_1, \dots, e_d\}$ . Consider the successive tensor powers  $E^{\otimes n}$  of  $E$  (equipped with some tensor norm). If one thinks of the elements  $e_i$  as letters, then  $E^{\otimes n}$  is spanned by the words of length  $n$  in the letters  $\{e_1, \dots, e_d\}$ , and can be identified with the space of real homogeneous non-commuting polynomials of degree  $n$  in  $d$  variables. We note that  $E^{\otimes 0} = \mathbb{R}$ .

**Definition A.1.** The space  $T((E))$  is defined to be the vector space of all formal  $E$ -tensors series.

**Definition A.2.** Let  $n \geq 1$  be an integer. Let  $B_n = \{\mathbf{a} = (a_0, a_1, \dots) | a_0 = \dots = a_n = 0\}$ . The truncated tensor algebra  $T^{(n)}(E)$  of order  $n$  over  $E$  is defined as the quotient algebra

$$T^{(n)}(E) = T((E)) / B_n. \quad (8)$$

The canonical homomorphism  $T((E)) \rightarrow T^{(n)}(E)$  is denoted by  $\pi_n$ .

In order for our analysis to work, we introduce the admissible norm of tensor powers defined as follows (the injective and projective norms, e.g.  $l_p$ -norm, satisfy our constraints).

**Definition A.3.** We say that the tensor powers of  $E$  are endowed with an admissible norm  $|\cdot|$ , if the following conditions hold:

1. For each  $n \geq 1$ , the symmetric group  $\mathcal{S}_n$  acts by isometry on  $E^{\otimes n}$ , i.e.

$$|\sigma v| = |v|, \forall v \in E^{\otimes n}, \forall \sigma \in \mathcal{S}_n$$

2. The tensor product has norm 1, i.e.  $\forall n, m \geq 1$ ,

$$|v \otimes w| \leq |v||w|, \forall v \in E^{\otimes n}, w \in E^{\otimes m}.$$

We introduce the  $p$ -variation as a measure of the roughness of the path.

**Definition A.4** ( $p$ -Variation). Let  $p \geq 1$  be a real number. Let  $X : J \rightarrow E$  be a continuous path. The  $p$ -variation of  $X$  on the interval  $J$  is defined by

$$\|X\|_{p,J} = \left[ \sup_{\mathcal{D} \subset J} \sum_{j=0}^{r-1} |X_{t_{j+1}} - X_{t_j}|^p \right]^{\frac{1}{p}}, \quad (9)$$

where the supremum is taken over any time partition of  $J$ , i.e.  $\mathcal{D} = (t_1, t_2, \dots, t_r)$ .<sup>2</sup>

Let  $\mathcal{C}^p(J, E)$  denote the range of any continuous path mapping from  $J$  to  $E$  of finite  $p$ -variation. The larger  $p$ -variation is, the rougher a path is. The compactness of the time interval  $J$  can't ensure the finite 1-variation of a continuous path in general. For example, Brownian motion has  $(2 + \varepsilon)$ -variation a.s  $\forall \varepsilon > 0$ , but it has infinite  $p$ -variation a.s.  $\forall p \in [1, 2]$ .

For each  $p \geq 1$ , the  $p$ -variation norm of a path  $X \in \mathcal{C}_p(J, E)$  is denoted by  $\|X\|_{p-var}$  and defined as follows:

$$\|X\|_{p-var} = \|X\|_{p,J} + \sup_{t \in J} \|X_t\|.$$

For concreteness, we state the decay rate of the signature for the path is of finite 1-variation. However, there is a similar statement of the factorial decay for the case of paths of finite  $p$ -variation [40].

<sup>2</sup> Let  $J = [s, t]$  be a closed bounded interval. A time partition of  $J$  is an increasing sequence of real numbers  $\mathcal{D} = (t_0, t_1, \dots, t_r)$  such that  $s = t_0 < t_1 < \dots < t_r = t$ . Let  $|\mathcal{D}|$  denote the number of time points in  $\mathcal{D}$ , i.e.  $|\mathcal{D}| = r + 1$ .  $\Delta \mathcal{D}$  denotes the time mesh of  $\mathcal{D}$ , i.e.  $\Delta \mathcal{D} := \max_{i=0}^{r-1} (t_{i+1} - t_i)$ .

**Lemma A.1** (Factorial Decay of the Signature). *Let  $X \in \mathcal{C}_1(J, E)$ . Then there exists a constant  $C > 0$ , such that for all  $m \geq 0$ ,*

$$|\pi_m(S(X))| \leq \frac{|X|_{1-var}^m}{m!}.$$

### A.1.2 Maximum Mean Discrepancy (MMD)

Maximum Mean Discrepancy (MMD) is a popular choice of distance between two distributions  $\mu$  and  $\nu$ , which can be used as the deterministic loss function in the context of the generative model. MMD is defined as

$$\text{MMD}(\mu, \nu) = \sup_{f \in \mathcal{H}} E_{X \sim \mu}[f(X)] - E_{X \sim \nu}[f(X)],$$

where  $\mathcal{H}$  denotes a Reproducing kernel Hilbert space (RKHS) with kernel  $k$ . RKHS is a Hilbert space of functionals  $\mathcal{X} \rightarrow \mathbb{R}$  endowed with the inner product and reproducing property and is rich enough to distinguish two measures. By the reproducing property of the kernel, MMD can be rewritten as

$$\text{MMD}(\mu, \nu) = \mathbb{E}_{X, X' \sim \mu}^{iid} [k(X, X')] - 2\mathbb{E}_{X \sim \mu, Y \sim \nu, X \sim Y}^{iid} [k(X, Y)] + \mathbb{E}_{Y, Y' \sim \nu}^{iid} [k(Y, Y')].$$

We implicitly assumed that  $(\mu, \nu)$  have required integrability properties for the right hand side to be finite. Due to this explicit representation MMD is very efficient to compute, but its performance in generative models depends on the choice of kernel  $k$  [3].

## A.2 The Signature Wasserstein-1 metric (Sig- $W_1$ )

In this subsection, we explain why the truncated Sig- $W_1$  metric can be used to approximate the conventional  $W_1$  metric on the measures on the path space. Then we give the detailed derivation on the explicit formula on the truncated Sig- $W_1$  metric (Lemma A.3).

Let us consider the space of time augmented paths  $\mathcal{X} = \Omega_0^1(J, E)$  defined in Section 2<sup>3</sup>, in which any discrete  $d$ -dimensional time series can be embedded using time augmentation and inserting the zero initial point (Definition 4.3, [27]).

Let  $K$  be a compact subset of  $\Omega_0^1(J, E)$  and  $\mu$  is a measure defined on  $K$ . For any  $X$  is sampled from  $\mu$ , the expected signature of  $X$  under the measure  $\mu$  is well defined and determines the measure on  $K$  uniquely [40]. By the definition of  $W_1(\mu, \nu)$ , there exists a sequence of  $f_n : K \rightarrow \mathbb{R}$  with bounded Lipschitz norm to attain the supremum  $W_1(\mu, \nu)$ . By the universality of the signature, it implies that  $\forall \epsilon > 0$ , for each  $f_n$ , there exists a linear functional  $L_n : T((E)) \rightarrow \mathbb{R}$  to approximate  $f_n$  uniformly, i.e.

$$\left| \int_K f_n(x) \mu(dx) - \int_K f_n(x) \nu(dx) - \left( \int_K L_n(S(x)) \mu(dx) - \int_K L_n(S(x)) \nu(dx) \right) \right| \leq 2\epsilon$$

Therefore we propose the Sig- $W_1$  metric on  $\mu$  and  $\nu$  by

$$\text{Sig-}W_1(\mu, \nu) = \sup_{|L| \leq 1, \text{ is a linear functional}} L(\mathbb{E}_\mu[S(x)] - \mathbb{E}_\nu[S(x)]),$$

where the Lipschitz  $L$  can be computed explicitly as  $L$  is a linear functional.

Next we give the error bound when restricting the linear functional  $L$  on the truncated signature in Lemma A.2 using the factorial decay of the signatures.

**Lemma A.2.** *Let  $L : T((E)) \rightarrow \mathbb{R}$  be a bounded linear functional, and  $K$  be a compact set of the range of the signature of a path in  $\mathcal{C}_0^1(J, E)$ . For any  $\epsilon > 0$ , there exists an integer  $M > 0$ ,*

$$\sup_{x \in K} |L(x) - L(\pi_M(x))| \leq \epsilon. \quad (10)$$

<sup>3</sup>To avoid the technical difficulties and highlight the main idea of our approach, we consider  $\Omega_0^1(J, E)$ . However, this assumption of the path space is strong. For example, Wiener measure is not defined on  $\Omega_0^1(J, E)$ . The condition may be relaxed if we embed the path of finite  $p$ -variation to the  $p$ -geometric rough path.

*Proof.* By Lemma A.1, for any  $x \in S$ , there exists  $l \in \mathcal{C}_1(J, E)$ ,

$$|x - \pi_M(x)| \leq \sum_{m \geq M} |\pi_m(x)| \leq \sum_{m \geq M} \frac{|l|_{1-var}^m}{m!} \leq \frac{|l|_{1-var}^{M+1}}{(M+1)!}. \quad (11)$$

As  $S$  is a compact set, therefore  $L := \sup_{S(l) \in S} |l|_{1-var}$  is bounded. It follows that

$$\lim_{M \rightarrow \infty} \frac{L^{M+1}}{(M+1)!} = 0,$$

which concludes the proof.  $\square$

Recall that the truncated Sig- $W_1$  norm of degree  $M$  is defined as for  $a = \mathbb{E}_\mu S_M(X) - \mathbb{E}_\nu S_M(X) \in T_M(E)$ ,

$$\sup\{L(a) | L \text{ is a linear functional on } T_M(E), \text{ and } |L| \leq 1\}. \quad (12)$$

When  $|L|$  is defined as the  $l_2$  norm of the linear coefficient vector induced by  $L$ , Equation (12) admits the solution  $|a|$  where  $|\cdot|$  is the  $l_2$  norm. The derivation boils down to the optimization problem in Lemma A.3.

**Lemma A.3.** Fix  $a \in \mathbb{R}^d$ . Let  $l^*$  denote the optimal  $l \in \mathbb{R}^d$  such as to maximize  $\langle l, a \rangle$  subject to  $|l| \leq 1$ . Then  $l^* = \frac{a}{|a|}$ , and  $\langle l^*, a \rangle = \sup_{|l| \leq 1} \langle l, a \rangle = |a|$ .

*Proof.* We apply the method of Lagrange multipliers to solve this problem. Let us consider the optimization problem  $U(l, \lambda) = \langle l, a \rangle + \lambda(|l|^2 - 1)$ . Then  $(l^*, \lambda^*)$  satisfies the following equation:

$$\begin{aligned} \partial_l U(l^*, \lambda) &= a - l^* \lambda = 0 \\ \partial_\lambda U(l^*, \lambda) &= |l^*|^2 - 1 = 0. \end{aligned}$$

It follows that  $\lambda = |a|$  and  $l^* = a/|a|$ , which implies that  $\langle l^*, a \rangle = |a|$ .  $\square$

### A.3 SigCWGAN

The core idea of SigCWGAN is to lift the time series to the signature feature as a principled and more effective feature extraction. In practice, the signature feature may often be accompanied with several following path transformations:

- Time jointed transformation ( Definition 4.3, [27] );
- Cumulative sum transformation: it is defined to map every  $(X_t)_{t=1}^T$  to  $CS_t := \sum_{i=1}^t X_i, \forall t \in \{1, \dots, T\}$  and  $CS_0 = \mathbf{0}$  ( Equation (2.20) in [26] ).
- Lead-Lag transformation ( Equation (2.8) in [26] ).
- Lag added transformation: The  $m$ -lag added transformation of  $(X_t)_{t=1}^T$  is defined as follows:  $\text{Lag}_m(X) = (Y_t)_{t=1}^{T-m}$ , such that

$$Y_t = (X_t, \dots, X_{t+m}).$$

Although in our analysis on the Sig- $W_1$  metric, we use the time augmented path to embed the discrete time series  $X$  to a continuous path for the ease of the discussion. However, to use Sig- $W_1$  metric to differentiate two measures on the path space, the only requirement of the way of embedding a discrete time series to a continuous path is that this embedding needs to ensure the bijection between the time series and its signature. Therefore, in practice we can choose other embedding to achieve that; for example, by applying the lead-lag transformation to time series, one can ensure the one-to-one correspondence between the time series and the signature.

The pseudocode of generating the next  $q$ -step forecast using  $G^\theta$  is given in Algorithm 1.

Pseudocode of SigCWGAN is listed in Algorithm 2.

---

**Algorithm 1** Pseudocode of Generating the next  $q$ -step forecast using  $G^\theta$ 


---

**Input:**  $x_{t-p+1:t}, G_\theta$   
**Output:**  $\hat{x}_{t+1:t+q}$   
1:  $\hat{x}_{\text{future}} \leftarrow$  a matrix of zeros of dimension  $d \times q$ .  
2:  $\hat{x} \leftarrow$  the concatenation of  $x_{t-p+1:t}$  and  $\hat{x}_{\text{future}}$ .  
3: **for**  $i = 1 : q$  **do**  
4:     We sample  $Z_i$  from the iid standard normal distribution.  
5:      $\hat{x}_{t+i} = G(\hat{x}_{t+i-p:t+i-1}, Z_i)$ .  
**return**  $\hat{x}_{t+1:t+q}$ .

---



---

**Algorithm 2** Pseudocode of SigCWGAN

---

**Input:**  $(x_t)_{t=1}^T$ , the signature degree of future path  $n$ , the signature degree of past path  $m$ , the length of future path  $q$ , the length of past path  $p$ , learning rate  $l$ , batch size  $B$   
**Output:**  $\theta$  - the optimal parameter of the AR-FNN generator  $G$   
1: We apply the path transformations to the past path and future path respectively and compute the corresponding the truncated signature  $(S_m(x_{t-p+1:t}), S_n(x_{t+1:t+q}))_t$ .  
2: Apply the linear regression on  $(S_m(x_{t-p+1:t}), S_n(x_{t+1:t+q}))_t$  and obtain the estimator of the linear function  $\hat{L}$ .  
3: Initialise the parameters  $\theta$  of the generator.  
4: **for**  $i = 1 : N$  **do**  
5:     We randomly select the set of time index of batch size  $B$ , denoted by  $\mathcal{T}$ .  
6:     **for**  $t \in \mathcal{T}$  **do**  
7:         We estimate the conditional signature under the measure  $\nu$ , i.e.

$$\hat{\mathbb{E}}_\nu[S_n(x_{t+1:t+q}))_t | x_{t-p+1:t}] = \hat{L}(S_m(x_{t-p+1:t})).$$

8:     Simulate  $n_{\text{MC}}$  samples of the simulated future path segments  $(\hat{x}^{(j)})_{j=1}^{n_{\text{MC}}}$  by the generator  $G^\theta$  given the past path  $x_{t-p+1:t}$  using Algorithm 1.  
9:     We estimate the conditional expected signature under the measure  $\mu$  induced by the generator as follows:

$$\hat{\mathbb{E}}_\mu[S_n(x_{t+1:t+q}))_t | x_{t-p+1:t}] = \frac{1}{n_{\text{MC}}} \sum_{j=1}^{n_{\text{MC}}} S_m(\hat{x}^{(j)}).$$

10:     Compute the loss function

$$L(\theta) = \frac{1}{\mathcal{T}} \sum_{t \in \mathcal{T}} |\hat{\mathbb{E}}_\nu[S_n(x_{t+1:t+q}))_t | x_{t-p+1:t}] - \hat{\mathbb{E}}_\mu[S_n(x_{t+1:t+q}))_t | x_{t-p+1:t}]|$$

11:      $\theta \leftarrow \theta - l \frac{dL(\theta)}{d\theta}$ .  
**return**  $\theta$ .

---

#### A.4 AR-FNN Architecture

We give a detailed description of the AR-FNN architecture below. For this purpose let us begin by defining the employed transformations, namely the parametric rectifier linear unit and the residual layer.

**Definition A.5** (Parametric rectifier linear unit). *The parametrised function  $\phi_\alpha \in C(\mathbb{R}, \mathbb{R})$ ,  $\alpha \geq 0$  defined as*

$$\phi_\alpha(x) = \max(0, x) + \alpha \min(0, x)$$

*is called parametric rectifier linear unit (PReLU).*

**Definition A.6** (Residual layer). *Let  $F : \mathbb{R}^n \rightarrow \mathbb{R}^n$  be an affine transformation and  $\phi_\alpha, \alpha \geq 0$  a PReLU. The function  $R : \mathbb{R}^n \rightarrow \mathbb{R}^n$  defined as*

$$R(x) = x + \phi_\alpha \circ F(x)$$

*where  $\phi_\alpha$  is applied component-wise, is called residual layer.*

The AR-FNN is defined as a composition of PReLUs, residual layers and affine transformations. Its inputs are the past  $p$ -lags of the  $d$ -dimensional process we want to generate as well as the  $d$ -dimensional noise vector. A formal definition is given below.

**Definition A.7 (AR-FNN).** *Let  $d, p \in \mathbb{N}$ ,  $A_1 : \mathbb{R}^{d(p+1)} \rightarrow \mathbb{R}^{50}$ ,  $A_4 : \mathbb{R}^{50} \rightarrow \mathbb{R}^d$  be affine transformations,  $\phi_\alpha, \alpha \geq 0$  a PReLU and  $R_2, R_3 : \mathbb{R}^{50} \rightarrow \mathbb{R}^{50}$  two residual layers. Then the function  $ArFNN : \mathbb{R}^{dp} \times \mathbb{R}^d \rightarrow \mathbb{R}^d$  defined as*

$$ArFNN(x, z) = A_4 \circ R_3 \circ R_2 \circ \phi_\alpha \circ A_1(xz)$$

where  $xz$  denotes the concatenated vectors  $x$  and  $z$ , is called autoregressive feedforward neural network (AR-FNN).

## A.5 Numerical Results

We use the following public codes for implementing the baselines:

- RCGAN: <https://github.com/ratschlab/RCGAN>
- Time-GAN: <https://github.com/jsyoon0823/TimeGAN>
- GMMN: <https://github.com/yujiali/gmmn>

For a fair comparison, we use the same neural network generator architecture, namely the 3-layer AR-FNN described in subsection A.4, for the SigCWGAN, TimeGAN, RCGAN and GMMN. The TimeGAN and RCGAN discriminators take as inputs the conditioning time series  $X_{1:p}$  concatenated with the synthetic time series  $X_{p+1:p+q}$ . Both discriminators use the AR-FNN as the underlying architecture. However, the first affine layer is adjusted such that the AR-FNN is defined as a function of the concatenated time series, i.e.  $p + q$  lags and not  $p$ -lags as for the generator. Similarly, the MMD is computed by concatenating the conditioning and synthetic time series. In order to obtain the bandwidth parameter for computing the MMD of the GMMN we benchmarked the median heuristic against using a mixture of bandwidths spanning multiple ranges as proposed in [38] and found latter to work best. In our experiments we used three kernels with bandwidths 0.1, 1, 5.

All algorithms were optimised for a total of 1,000 generator weight updates. The neural network weights were optimised by using the Adam optimiser [41] and learning rates for the generators were set to 0.001. For the RCGAN and TimeGAN we applied two time-scale updates (TTUR) [42] and set the learning rate to 0.003. Furthermore, we updated the discriminator's weights two times per generator weight update in order to improve convergence of the GAN.

In our numerical experiments, to compute the signature for the SigCWGAN method, we choose to apply the following path transformations on the time series before computing the signatures: (1) we combine the path  $x_{\text{past}}$  with its cumulative sum transformed path, denoted by  $y_{\text{past}}$ , which is a  $2d$ -dimensional path; (2) we apply 1-lag added transformation on  $y_{\text{past}}$ ; (3) it follows with the Lead-Lag transformation. The signature of such transformed path can well capture the marginal distributions, auto-correlations and other temporal characteristics of the time-series data.

In the following, we describe the calculation of the test metrics precisely. Let  $(X_t)_{t=1}^T$  denote a  $d$ -dimensional time series sampled from the real target distribution. We first extract the input-out pairs  $(X_{t-p+1:t}, X_{t+1:t+q})_{t \in \mathcal{T}}$ , where  $\mathcal{T}$  is the set of time indexes. Given the generator  $G$ , for each input sample  $(X_{t-p+1:t})$ , we generate one sample of the  $q$ -step forecast  $\hat{X}_{t+1,t+q}^{(t)}$  (if  $G$  is not conditional generator, we generate a sample of  $q$ -step forecast  $\hat{X}_{t+1,t+q}^{(t)}$  without any conditioning variable.). The synthetic data generated by  $G$  is given by  $(\hat{X}_{t+1,t+q}^{(t)})_t$ , which we use to compute the test metrics.

**Metric on marginal distribution** Following [21], we use  $(X_{t+1:t+q})_{t \in \mathcal{T}}$  and  $(\hat{X}_{t+1:t+q}^{(t)})_{t \in \mathcal{T}}$  as the samples of the marginal distribution of the real data and synthetic data per each time step. For each feature dimension  $i \in \{1, \dots, d\}$ , we compute two empirical density functions based on the histograms of the real data and synthetic data resp. denoted by  $\hat{df}_r^i$  and  $\hat{df}_G^i$ . Then the metric on marginal distribution of the true and synthetic data is given by

$$\frac{1}{d} \sum_{i=1}^d |\hat{df}_r^i - \hat{df}_G^i|_1.$$



**Absolute difference of lag-1 auto-correlation** The auto-covariance of  $i^{th}$  feature of the real data with lag value  $k$  is computed by

$$\rho_r^i(k) := \frac{1}{T-k} \sum_{t=1}^{T-k} (X_t^i - \bar{X}^i)(X_{t+k}^i - \bar{X}^i),$$

where  $\bar{X}^i$  is the average of  $(X_t^i)_{t=1}^T$ .

For the synthetic data, we estimate the auto-covariance of  $i^{th}$  feature with lag value  $k$  is computed by

$$\rho_G^i(k) := \frac{1}{|\mathcal{T}|} \sum_{t=1}^{|\mathcal{T}|} \hat{X}_{t+1}^{(t),i} \hat{X}_{t+k}^{(t),i} - \left( \frac{1}{|\mathcal{T}|} \sum_{t=1}^{|\mathcal{T}|} \hat{X}_{t+1}^{(t),i} \right) \left( \frac{1}{|\mathcal{T}|} \sum_{t=1}^{|\mathcal{T}|} \hat{X}_{t+k}^{(t),i} \right). \quad (13)$$

The estimator of the lag-1 auto-correlation of the real/synthetic data is given by  $\frac{\rho_r^i(1)}{\rho_r^i(0)} / \frac{\rho_G^i(1)}{\rho_G^i(0)}$ . The ACF score is defined to be the absolute difference of lag-1 auto-correlation given as follows:

$$\frac{1}{d} \sum_{i=1}^d \left| \frac{\rho_r^i(1)}{\rho_r^i(0)} - \frac{\rho_G^i(1)}{\rho_G^i(0)} \right|.$$

**Metric on the correlation** We estimate the covariance of the  $i^{th}$  and  $j^{th}$  feature of time series from the true data as follows:

$$\text{cov}_r^{i,j} = \frac{1}{T} \sum_{t=1}^T X_t^i X_t^j - \left( \frac{1}{T} \sum_{t=1}^T X_t^i \right) \left( \frac{1}{T} \sum_{t=1}^T X_t^j \right).$$

Similarly, we estimate the covariance of the  $i^{th}$  and  $j^{th}$  feature of time series from the synthetic data by

$$\text{cov}_G^{i,j} = \frac{1}{|\mathcal{T}|} \frac{1}{q} \sum_{t=1}^{|\mathcal{T}|} \sum_{s=1}^q \hat{X}_{t+s}^{(t),i} \hat{X}_{t+s}^{(t),j} - \left( \frac{1}{|\mathcal{T}|} \sum_{t \in \mathcal{T}} \hat{X}_{t+s}^{(t),i} \right) \left( \frac{1}{|\mathcal{T}|} \sum_{t \in \mathcal{T}} \hat{X}_{t+s}^{(t),j} \right).$$

Thus the estimator of the correlation of the  $i^{th}$  and  $j^{th}$  feature of time series from the real/synthetic data are given by  $\tau_r^{i,j} := \frac{\text{cov}_r^{i,j}}{\sqrt{\text{cov}_r^{i,i} \text{cov}_r^{j,j}}}$  and  $\tau_G^{i,j} := \frac{\text{cov}_G^{i,j}}{\sqrt{\text{cov}_G^{i,i} \text{cov}_G^{j,j}}}$ . Then the metric on the correlation between the real data and synthetic data is given by  $l_1$  norm of the difference of two correlation matrices  $(\tau_r^{i,j})_{i,j \in \{1, \dots, d\}}$  and  $(\tau_G^{i,j})_{i,j \in \{1, \dots, d\}}$ .

**TRTR/TSTR  $R^2$**  We split the input-output pairs  $(X_{t-p+1:t}, X_{t+1})$  from the real data into the train set and test set. We apply the linear signature model on real training data  $(X_{t-p+1:t}, X_{t+1})$ , validate it and compute the corresponding  $R^2$  on the on the real test data (TRTR  $R^2$ ). Then we apply the same linear signature model on the synthetic data  $(X_{t-p+1:t}, \hat{X}_{t+1})$ , where  $\hat{X}_{t+1}$  is simulated by the generator conditioning on the  $X_{t-p+1:t}$ . We evaluate the trained model on the real test data and corresponding  $R^2$  is called (TSTR  $R^2$ ).

### A.5.1 VAR(1)

We conduct the extensive experiments on VAR(1) with different hyper-parameter settings, i.e.  $d \in \{1, 2, 3\}$ ,  $\sigma, \phi \in \{0.2, 0.5, 0.8\}$ . The numerical results for VAR(1) synthetic data are summarized in Table 2, 3 and 4. We highlight the best results with respect to each test metric in bold.

Table 2: Numerical results of VAR(1) for  $d = 1$ 

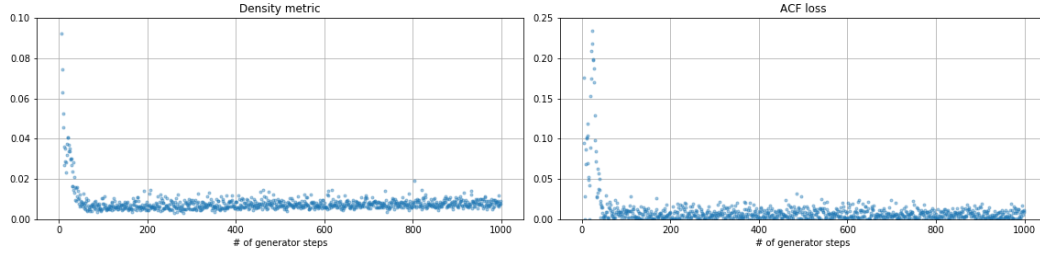
Settings	Temporal Correlations		
	$\phi = 0.2$	$\phi = 0.5$	$\phi = 0.8$
Metric on marginal distribution			
SigCWGAN	0,0118	0,0101	0,0070
TimeGAN	0,0244	0,0259	0,0127
RCGAN	0,0133	<b>0,0065</b>	<b>0,0049</b>
GMMN	<b>0,0064</b>	<b>0,0065</b>	0,0055
Absolute difference of lag-1 autocorrelation			
SigCWGAN	0,0067	<b>0,0019</b>	<b>0,0029</b>
TimeGAN	<b>0,0027</b>	0,0499	0,0086
RCGAN	0,0408	0,0378	0,0106
GMMN	0,0173	0,0048	0,0140
$R^2$ obtained from TSTR. (TRTR first row.)			
TRTR	0,0510	0,2625	0,6418
SigCWGAN	0,0502	0,2614	<b>0,6413</b>
TimeGAN	0,0479	0,2541	0,6391
RCGAN	<b>0,0506</b>	<b>0,2622</b>	0,6404
GMMN	0,0501	0,2603	0,6307
Sig- $W_1$ distance			
SigCWGAN	<b>0,1029</b>	<b>0,0846</b>	<b>0,0552</b>
TimeGAN	0,3845	0,2851	0,1766
RCGAN	0,2268	0,1695	0,1201
GMMN	0,1441	0,1337	0,2306

Table 3: Numerical results of VAR(1) for  $d = 2$ 

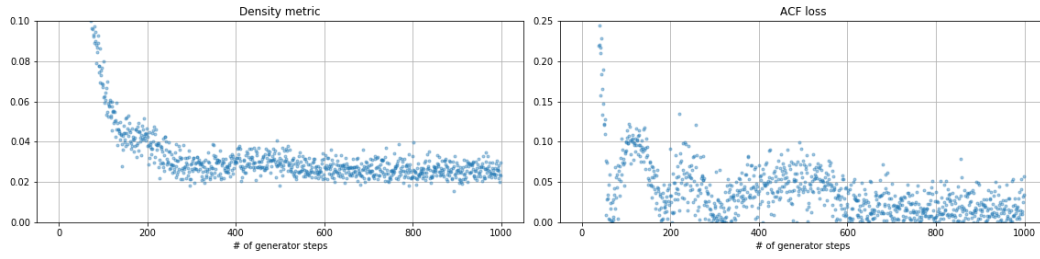
Temporal Correlations (fixing $\sigma = 0.8$ )    Feature Correlations (fixing $\phi = 0.8$ )						
Settings	$\phi = 0.2$	$\phi = 0.5$	$\phi = 0.8$	$\sigma = 0.2$	$\sigma = 0.5$	$\sigma = 0.8$
Metric on marginal distribution						
SigCWGAN	0,0078	0,0083	0,0059	0,0063	<b>0,0054</b>	0,0059
TimeGAN	0,0209	0,0211	0,0092	0,0159	0,0163	0,0092
RCGAN	<b>0,0061</b>	0,0120	0,0080	0,0071	0,0122	0,0820
GMMN	0,0067	<b>0,0082</b>	<b>0,0053</b>	<b>0,0053</b>	<b>0,0054</b>	<b>0,0053</b>
Absolute difference of lag-1 autocorrelation						
SigCWGAN	<b>0,0123</b>	<b>0,0063</b>	<b>0,0027</b>	<b>0,0010</b>	<b>0,0016</b>	<b>0,0027</b>
TimeGAN	0,0536	0,0978	0,0366	0,1115	0,0916	0,0366
RCGAN	0,0169	0,0209	0,0527	0,0722	0,0271	0,0527
GMMN	0,0190	0,0500	0,0336	0,0766	0,0526	0,0336
$L_1$ -norm of real and generated cross correlation matrices						
SigCWGAN	<b>0,0073</b>	<b>0,0121</b>	<b>0,0087</b>	<b>0,0136</b>	<b>0,0131</b>	<b>0,0087</b>
TimeGAN	0,0234	0,0557	0,0501	0,0851	0,1965	0,0501
RCGAN	0,0962	0,2091	0,0321	0,0225	0,0753	0,0321
GMMN	0,0096	0,0135	0,0187	0,0415	0,0275	0,0187
$R^2$ obtained from TSTR. (TRTR first row.)						
TRTR	0,0393	0,2498	0,6480	0,6450	0,6465	0,6480
SigCWGAN	<b>0,0383</b>	<b>0,2482</b>	<b>0,6475</b>	<b>0,6443</b>	<b>0,6459</b>	<b>0,6475</b>
TimeGAN	0,0263	0,2333	0,5823	0,6163	0,6031	0,5823
RCGAN	0,0167	0,1987	0,5763	0,6304	0,6203	0,6359
GMMN	0,0228	0,2138	0,6093	0,5754	0,5846	0,6093
Sig- $W_1$ distance						
SigCWGAN	<b>0,2500</b>	<b>0,2013</b>	<b>0,1346</b>	<b>0,1358</b>	<b>0,1363</b>	<b>0,1346</b>
TimeGAN	0,6853	0,5377	0,5495	0,6392	0,6321	0,5495
RCGAN	0,4253	0,6706	0,6922	0,7832	0,6038	0,6922
GMMN	0,3879	0,4081	0,527	0,7057	0,6507	0,5271

Table 4: Numerical results of VAR(1) for  $d = 3$ 

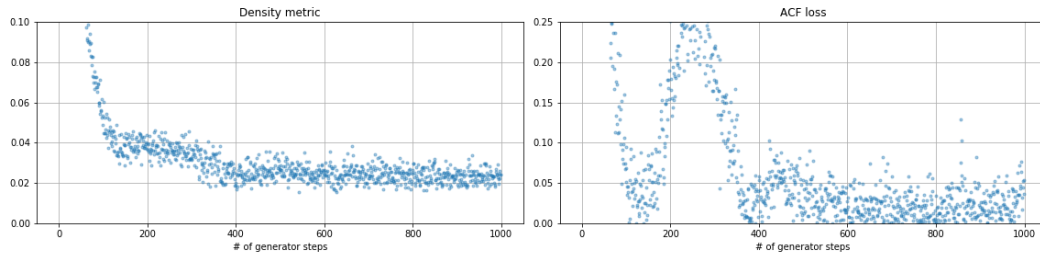
Temporal Correlations (fixing $\sigma = 0.8$ )    Feature Correlations (fixing $\phi = 0.8$ )						
Settings	$\phi = 0.2$	$\phi = 0.5$	$\phi = 0.8$	$\sigma = 0.2$	$\sigma = 0.5$	$\sigma = 0.8$
Metric on marginal distribution						
SigCWGAN	<b>0,0065</b>	<b>0,0069</b>	<b>0,0053</b>	<b>0,0043</b>	<b>0,0050</b>	<b>0,0053</b>
TimeGAN	0,0269	0,0220	0,0100	0,0131	0,0105	0,0100
RCGAN	0,0077	0,0080	0,0078	0,0093	0,0082	0,0078
GMMN	0,0081	0,0081	0,0072	0,0108	0,0109	0,0072
Absolute difference of lag-1 autocorrelation						
SigCWGAN	<b>0,0122</b>	<b>0,0050</b>	<b>0,0024</b>	<b>0,0024</b>	<b>0,0037</b>	<b>0,0024</b>
TimeGAN	0,0578	0,0559	0,0796	0,0319	0,0245	0,0796
RCGAN	0,0298	0,0741	0,0355	0,0888	0,1069	0,0355
GMMN	0,0340	0,0582	0,0977	0,0947	0,1200	0,0977
$L_1$ -norm of real and generated cross correlation matrices						
SigCWGAN	<b>0,0065</b>	<b>0,0026</b>	<b>0,0059</b>	<b>0,0165</b>	<b>0,0110</b>	<b>0,0059</b>
TimeGAN	0,2301	0,5181	0,2475	0,1201	0,2235	0,2475
RCGAN	0,1489	0,2610	0,2118	0,0981	0,2917	0,2118
GMMN	0,0707	0,1107	0,1820	0,2246	0,3934	0,1820
$R^2$ obtained from TSTR. (TRTR first row.)						
TRTR	0,441	0,2601	0,6519	0,6515	0,6517	0,6519
SigCWGAN	<b>0,0401</b>	<b>0,2580</b>	<b>0,6511</b>	<b>0,6503</b>	<b>0,6508</b>	<b>0,6511</b>
TimeGAN	0,0100	0,2064	0,6091	0,6305	0,6140	0,6091
RCGAN	0,0266	0,2043	0,5951	0,5915	0,5855	0,5951
GMMN	-0,0099	0,1711	0,5342	0,4955	0,5017	0,5342
Sig- $W_1$ distance						
SigCWGAN	<b>0,5011</b>	<b>0,3970</b>	<b>0,2688</b>	<b>0,2664</b>	<b>0,2681</b>	<b>0,2688</b>
TimeGAN	1,2627	1,0881	0,8851	0,8467	0,9126	0,8851
RCGAN	0,7411	0,9273	0,9599	1,1650	1,1130	0,9599
GMMN	0,8352	0,8492	0,9873	1,2482	1,2047	0,9873



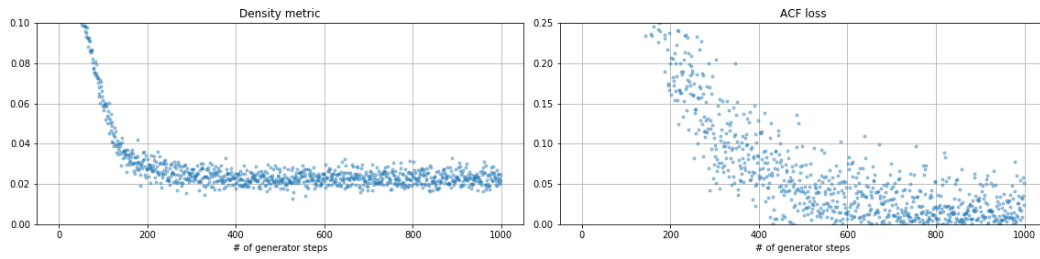
(a) SigCWGAN



(b) TimeGAN

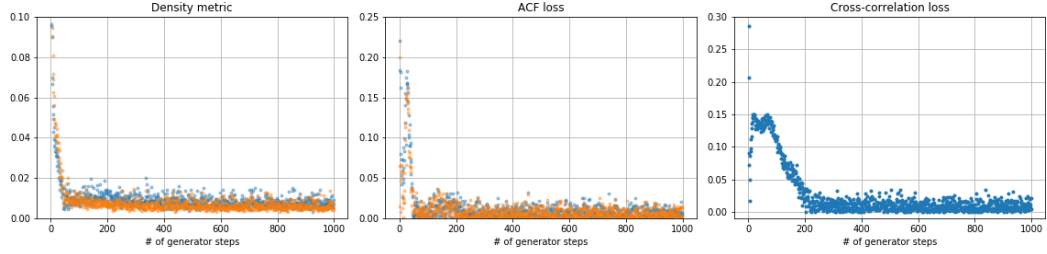


(c) RCGAN

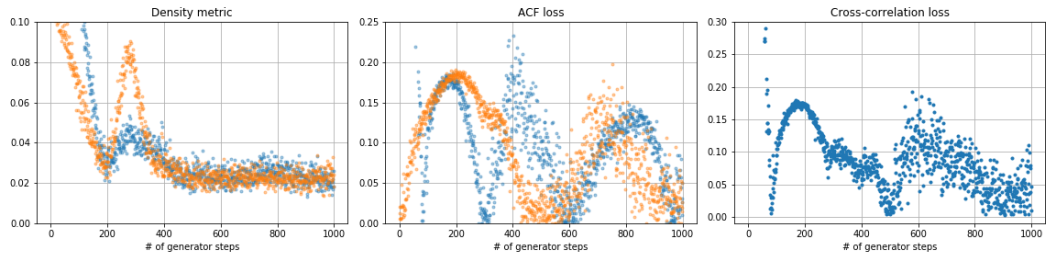


(d) GMMN

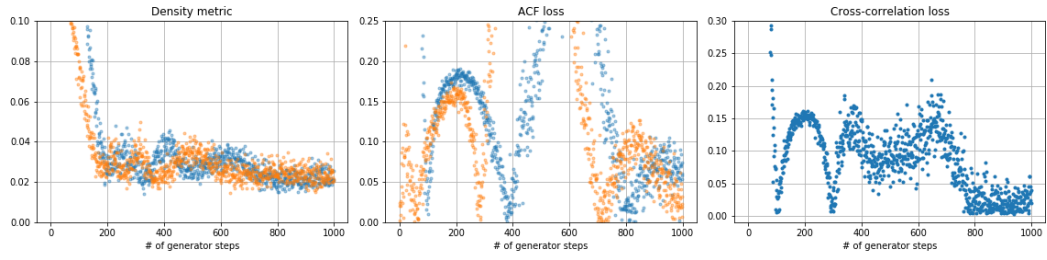
Figure 6: Exemplary development of the considered distances and score functions during training for the 1-dimensional VAR(1) model with autocorrelation coefficient  $\phi = 0.8$ .



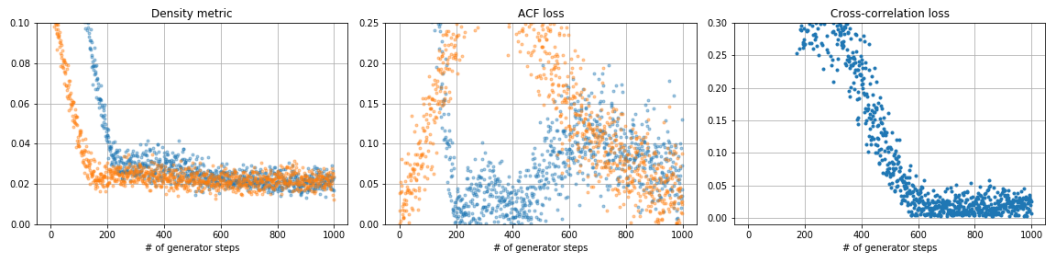
(a) SigCWGAN



(b) TimeGAN

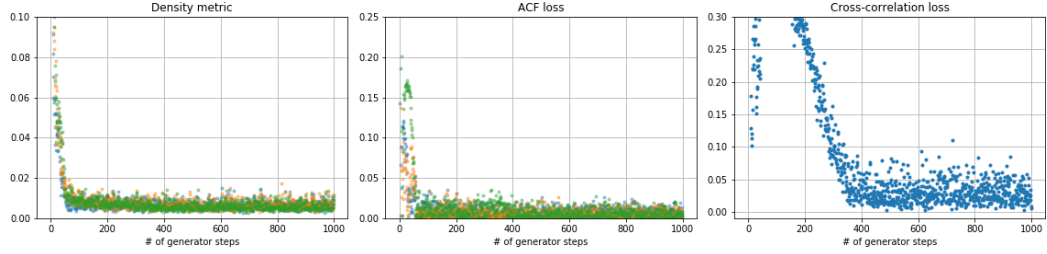


(c) RCGAN

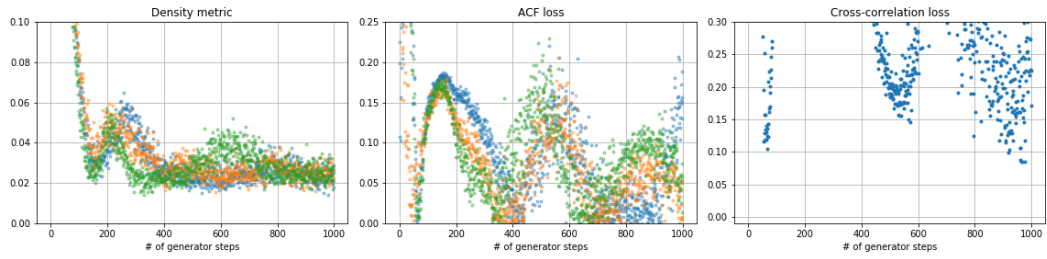


(d) GMMN

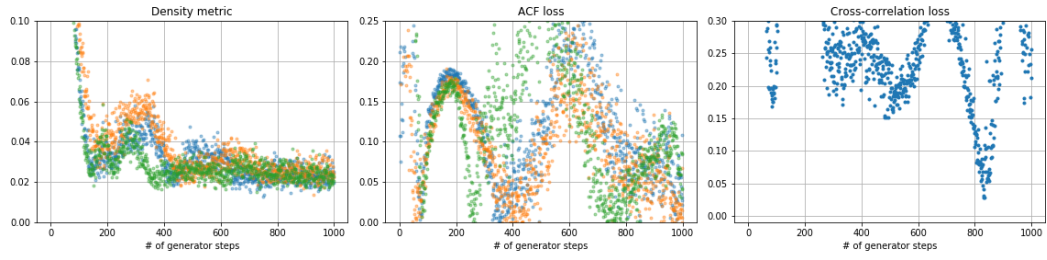
Figure 7: Exemplary development of the considered distances and score functions during training for the 2-dimensional VAR(1) model with autocorrelation coefficient  $\phi = 0.8$  and co-variance parameter  $\sigma = 0.8$ . The colours blue and orange indicate the relevant distance / score for each dimension.



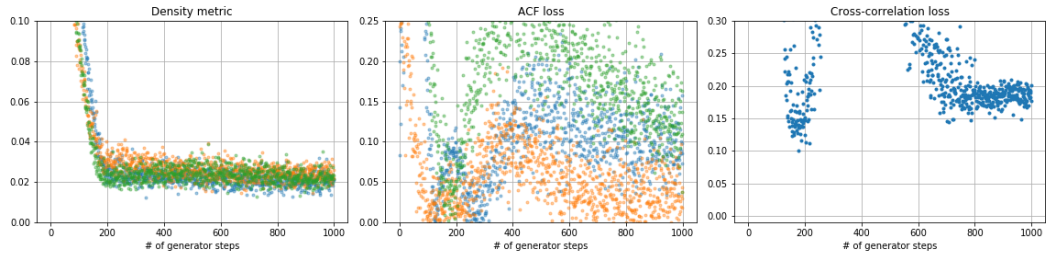
(a) SigCWGAN



(b) TimeGAN



(c) RCGAN



(d) GMMN

Figure 8: Exemplary development of the considered distances and score functions during training for the 3-dimensional VAR(1) model with autocorrelation coefficient  $\phi = 0.8$  and co-variance parameter  $\sigma = 0.8$ . The colours blue, orange and green indicate the relevant distance / score for each dimension.

For  $d = 3, \phi = 0.8, \sigma = 0.8$ , the comparison results of the test metrics on the marginal distribution and auto-correlation are given in Table 9. Figure 10 proves that the SigCWGAN can produce the synthetic data to capture the feature correlation of time series better than the other baselines.

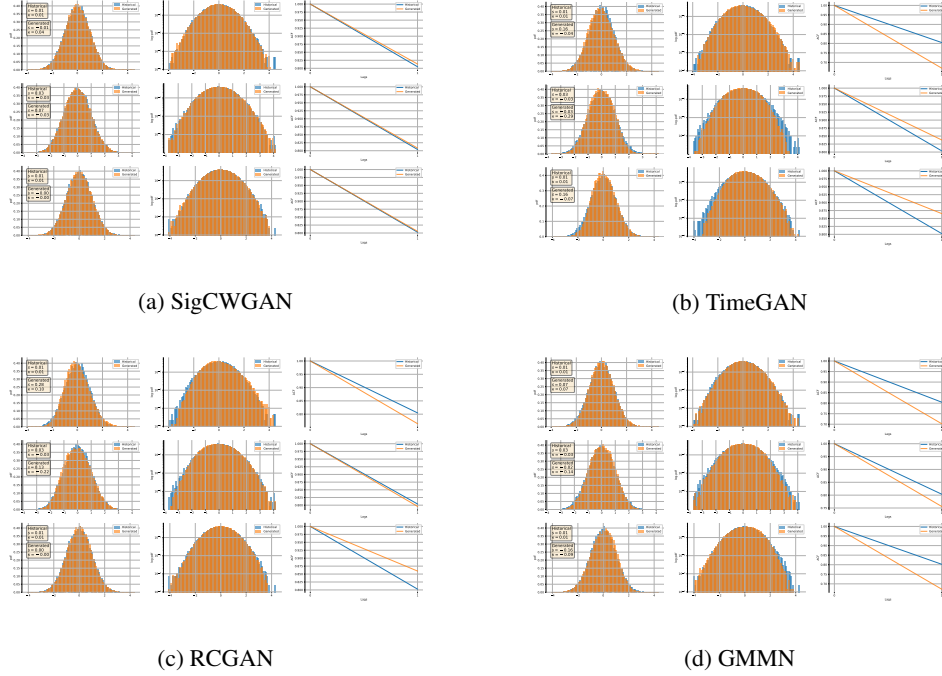


Figure 9: The plot of the marginal distribution on the linear scale (1st column), log-scale (2nd column) and the auto-correlation fit of the first lag (3rd column) for the  $d = 3$ -dimensional VAR(1) model with autocorrelation coefficient  $\phi = 0.8$  and co-variance parameter  $\sigma = 0.8$ . The orange bars in the first two columns display the generated PDF, whereas the PDF of the real distribution is displayed in blue. Similarly, the orange lines in the plot of the auto-correlation fit display the generated autocorrelation, whereas the real auto-correlation is displayed in blue. The synthetic data from which marginals and auto-correlations were computed was obtained by generating recurrently  $q = 3$  steps ahead.

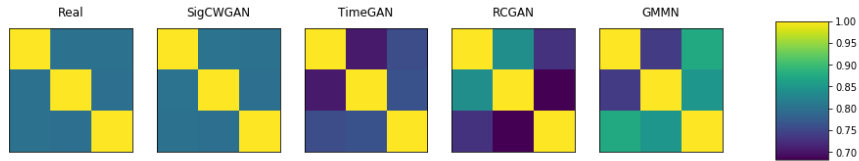
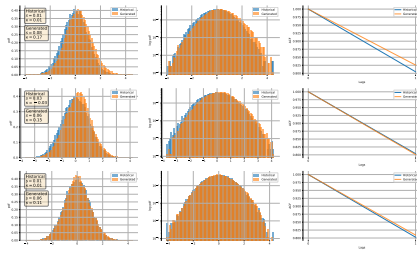
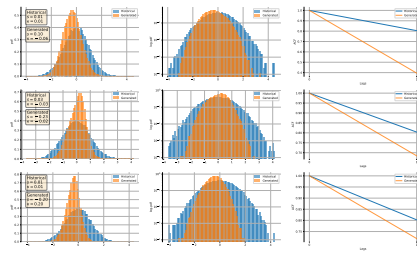


Figure 10: The plot of correlation fitting for VAR(1) model with autocorrelation coefficient  $\phi = 0.8$  and co-variance parameter  $\sigma = 0.8$ .

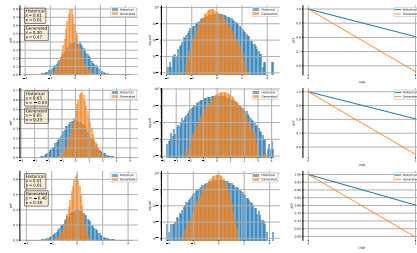




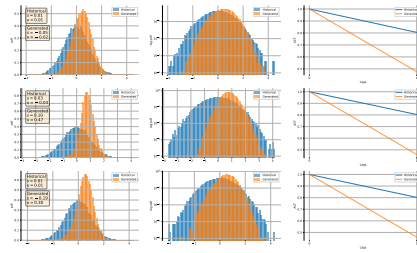
(a) SigCWGAN



(b) TimeGAN



(c) RCGAN



(d) GMMN

Figure 11: The plot of the marginal distribution and the auto-correlation fitting for VAR(1) model with autocorrelation coefficient  $\phi = 0.8$  and co-variance parameter  $\sigma = 0.8$ . The synthetic data from which marginals and auto-correlations were computed was obtained by generating recurrently a single path for 80.000 steps. Visually, the marginals and auto-correlations of the baseline models do not fit the real distribution well, whereas the SigCWGAN gives a good fit.

### A.5.2 ARCH(p)

We implement extensive experiments on ARCH(p) with different  $p$ -lag values, i.e.  $p \in \{2, 3, 4\}$ . The numerical results are summarized in Table 5. The best results among all the models are highlighted in bold.

Table 5: Numerical results of the ARCH(p) datasets.

Settings	$p = 2$	$p = 3$	$p = 4$
Metric on marginal distribution			
SigCWGAN	0,00918	0,00880	<b>0.01142</b>
TimeGAN	0,02569	0,02119	0.2191
RCGAN	0,01069	0,01612	0.01182
GMMN	<b>0,00744</b>	<b>0,00783</b>	0.01259
Absolute difference of lag-1 autocorrelation			
SigCWGAN	<b>0,00542</b>	<b>0,00852</b>	<b>0.01106</b>
TimeGAN	0,01714	0,02401	0.03267
RCGAN	0,05372	0,01685	0.04879
GMMN	0,02056	0,00859	0.01441
$L_1$ -norm of real and generated cross correlation matrices			
SigCWGAN	0,00462	<b>0,00546</b>	0.00489
TimeGAN	<b>0,00315</b>	0,06551	0.04408
RCGAN	0,01604	0,08823	<b>0.00235</b>
GMMN	0,04326	0,03930	0.01603
$R^2$ obtained from TSTR. (TRTR first row.)			
TRTR	0,32168	0,32615	0.33305
SigCWGAN	<b>0,31623</b>	<b>0,31913</b>	<b>0.31642</b>
TimeGAN	0,30835	0,30556	0.30240
RCGAN	0,31146	0,30727	0.30924
GMMN	0,27982	0,28072	0.30742
Sig- $W_1$ distance			
SigCWGAN	<b>0,12210</b>	<b>0,14682</b>	<b>0.14098</b>
TimeGAN	0,20228	0,22761	0.23398
RCGAN	0,18781	0,20943	0.21876
GMMN	0,26797	0,26853	0.25811

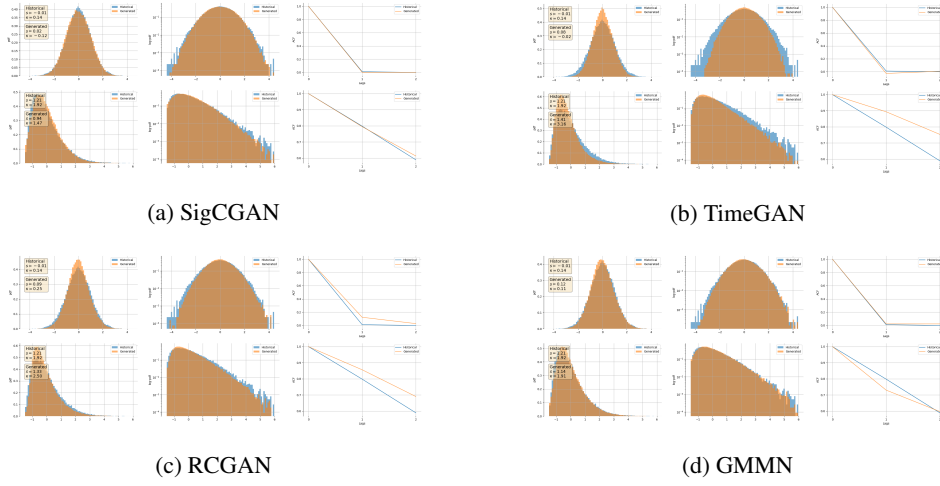
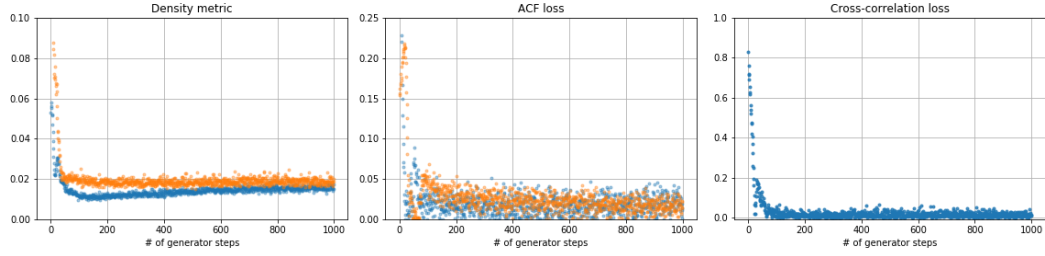


Figure 12: The plot displays a comparison of the marginal distribution on the linear- and log-scale, as well as the fit of the auto-correlation for ARCH(3) data. Histograms and the auto-correlation of the data is indicated in blue and the fits from the generator are coloured in orange.

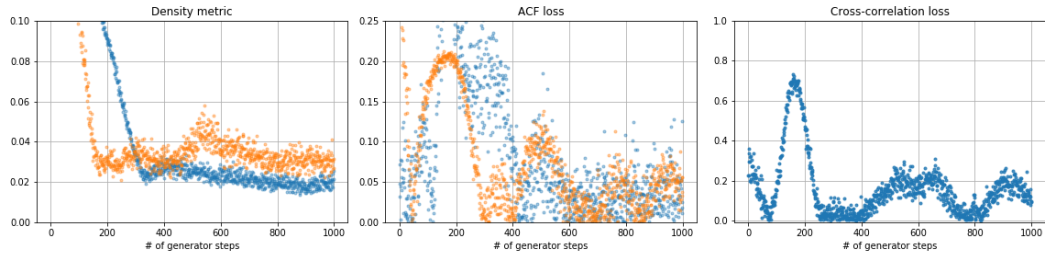
### A.5.3 Empirical Data

Table 6: Numerical results of the stocks datasets.

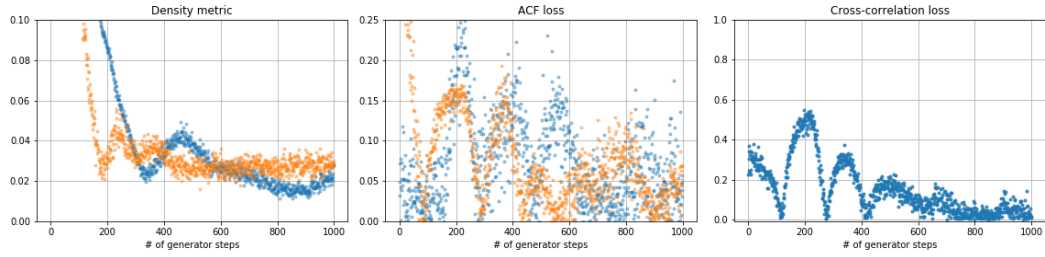
Data type	SPX		SPX + DJI
Metric on marginal distribution			
SigCWGAN	0,01730		0,01674
TimeGAN	0,02155		0,02127
RCGAN	0,02094		<b>0,01655</b>
GMMN	<b>0,01608</b>		0,02387
Absolute difference of lag-1 autocorrelation			
SigCWGAN	0,01342		<b>0,01192</b>
TimeGAN	0,05792		0,03035
RCGAN	0,03362		0,04075
GMMN	<b>0,01283</b>		0,02676
$L_1$ -norm of real and generated cross correlation matrices			
SigCWGAN	<b>0,01079</b>		<b>0,07435</b>
TimeGAN	0,12363		0,61488
RCGAN	0,04606		0,15353
GMMN	0,04651		0,22380
$R^2$ obtained from TSTR. (TRTR first row.)			
TRTR	0,31706		0,31934
SigCWGAN	0,30797		0,29396
TimeGAN	0,29818		0,29192
RCGAN	<b>0,30822</b>		<b>0,29638</b>
GMMN	0,28837		0,29576
Sig- $W_1$ distance			
SigCWGAN	<b>0,31775</b>		<b>4,36744</b>
TimeGAN	0,58541		5,99482
RCGAN	0,47107		5,43254
GMMN	0,59073		6,23777



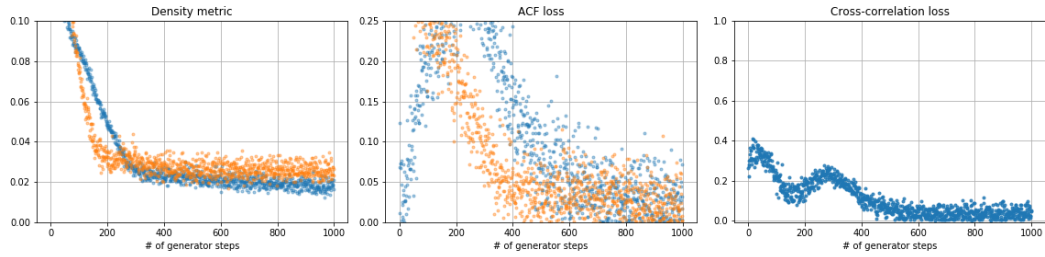
(a) SigCWGAN



(b) TimeGAN

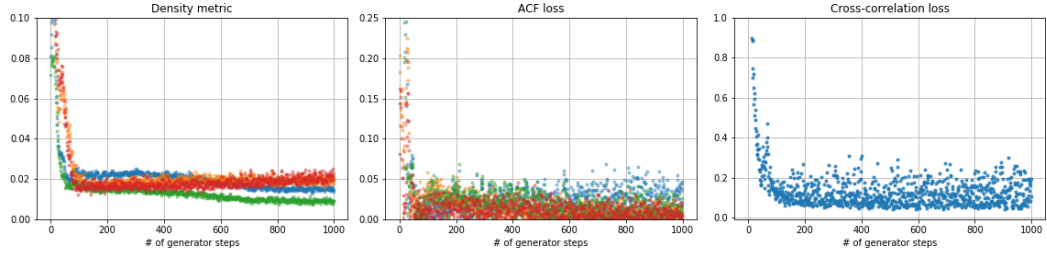


(c) RCGAN

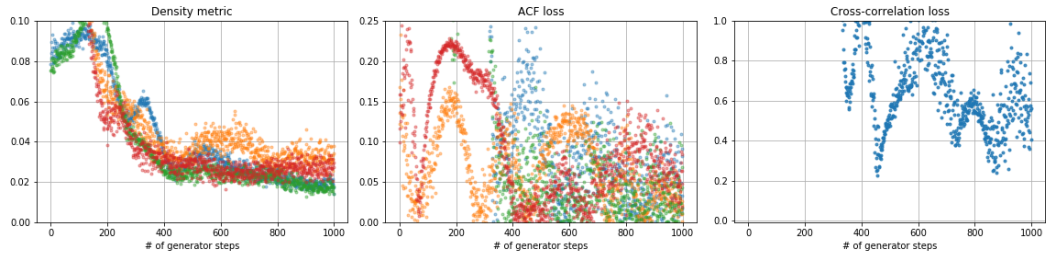


(d) GMMN

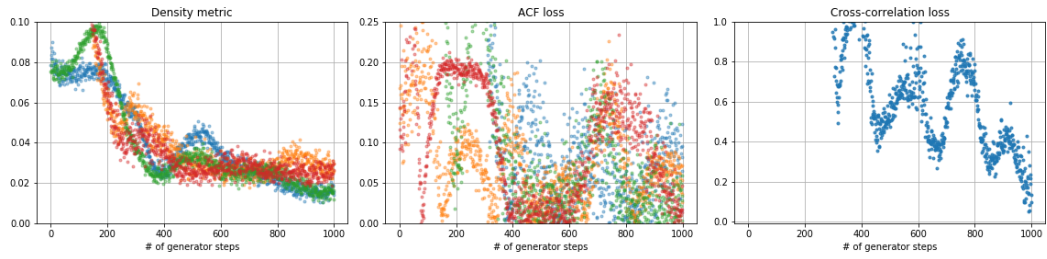
Figure 13: Exemplary development of the considered distances and score functions during training for SPX data.



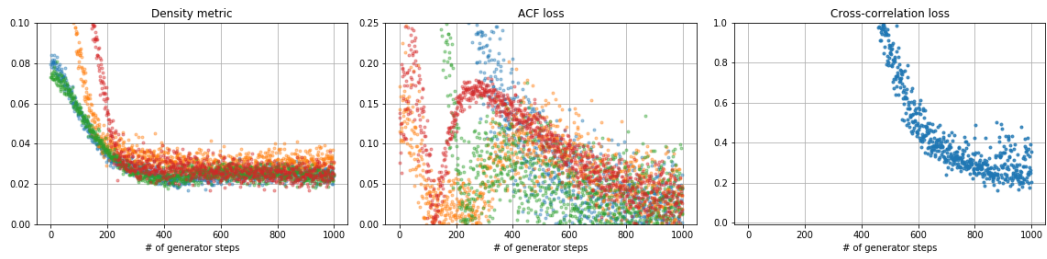
(a) SigCWGAN



(b) TimeGAN



(c) RCGAN



(d) GMMN

Figure 14: Exemplary development of the considered distances and score functions during training for SPX and DJI data.

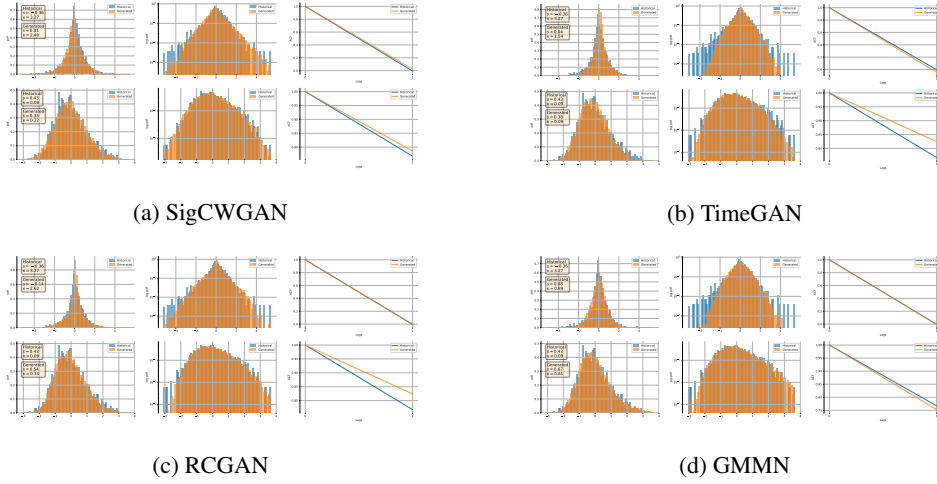
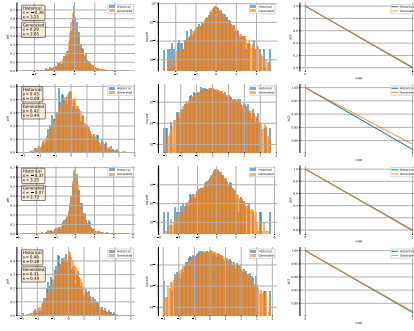


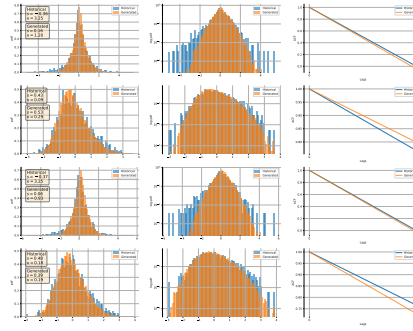
Figure 15: The plot displays a comparison of the marginal distribution on the linear- and log-scale, as well as the fit of the auto-correlation for SPX data. Histograms and the auto-correlation of the data is indicated in blue and the fits from the generator are coloured in orange.



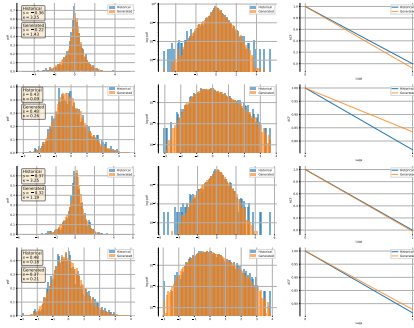
Figure 16: Comparison of real and synthetic cross-correlation matrices for SPX data. On the far left the real cross-correlation matrix from SPX log-return and log-volatility data is shown. The colorbar on the right indicates the range of values taken. Observe that the historical correlation between log-returns and log-volatility is negative, indicating the presence of leverage effects, i.e. when log-returns are negative, log-volatility is high.



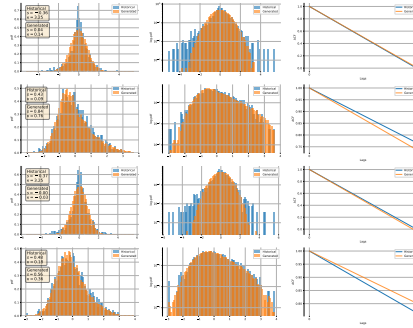
(a) SigCWGAN



(b) TimeGAN



(c) RCGAN



(d) GMMN

Figure 17: The plot displays a comparison of the marginal distribution on the linear- and log-scale, as well as the fit of the auto-correlation for SPX and DJI data. Histograms and the auto-correlation of the data is indicated in blue and the fits from the generator are colored in orange.

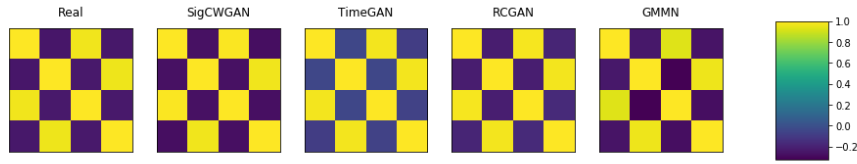


Figure 18: Comparison of real and synthetic cross-correlation matrices for SPX and DJI log-return and log-volatility data. On the far left the real cross-correlation matrix from SPX and DJI data is shown. The colorbar on the far right indicates the range of values taken.